Origin of dimethylsulfide, non-sea-salt sulfate, and methanesulfonic acid in eastern Antarctica

E. Cosme[1]
Laboratoire de Glaciologie et Géophysique de l'Environnement, Saint-Martin-d'Hères, France

F. Hourdin
Laboratoire de Météorologie Dynamique, CNRS – Université Pierre et Marie Curie, Paris, France

C. Genthon and P. Martinerie
Laboratoire de Glaciologie et Géophysique de l'Environnement, Saint-Martin-d'Hères, France

Received 8 April 2004; revised 13 July 2004; accepted 25 October 2004; published 8 February 2005.

[1] Ignoring the origin of atmospheric chemicals is often a strong limitation to the full interpretation of their measurement. In this article, this question is addressed in the case of the sulfur species in Antarctica, with an original method of retrotransport of tracers. The retrotransport model is derived from the Laboratoire de Météorologie Dynamique Zoom-Tracers (LMD-ZT) atmospheric general circulation model, optimized for polar climate and expanded to simulate atmospheric sulfur chemistry. For two East Antarctic scientific stations (Dumont d'Urville and Vostok) the effects of transport and chemistry and the influence of oceanic, volcanic, and anthropogenic sources on dimethylsulfide (DMS), non-sea-salt (nss) sulfate, and methanesulfonic acid (MSA) concentrations are evaluated in summer and winter. The oceanic source largely dominates, but other sources can episodically be significant. The meridional origin and the age of DMS, MSA, and biogenic nss sulfate are also estimated. The latitudes of origin of MSA and nss sulfate are similar in summer, but they differ markedly in winter. This is a signature of their different chemical production scheme. Also, the interannual variability of the origin of the sulfur species at Vostok is weak compared to that at Dumont d'Urville. Acknowledging that the DMS concentrations in the ocean have no interannual variability in the model, this result suggests unsurprisingly that inland Antarctic stations may be better observation sites to monitor large-scale DMS bioproductivity variability than coastal sites are. The combination of slower chemistry and more intense atmospheric circulation in winter leads to unexpected results, such as a younger DMS in winter than in summer at Vostok.

Citation: Cosme, E., F. Hourdin, C. Genthon, and P. Martinerie (2005), Origin of dimethylsulfide, non-sea-salt sulfate, and methanesulfonic acid in eastern Antarctica, *J. Geophys. Res.*, *110*, D03302, doi:10.1029/2004JD004881.

1. Introduction

[2] Aerosols may efficiently affect climate by their interaction with solar radiation, either directly [*McCormick and Ludwig*, 1967; *Shaw*, 1983] or indirectly, i.e., acting as cloud condensation nuclei (CCN) [*Twomey*, 1974; *Albrecht*, 1989; *Boucher and Lohmann*, 1995]. In marine unpolluted regions, the CCN number concentration is dominated by non-sea-salt sulfate aerosols [*Charlson et al.*, 1987]. The main primary precursor of sulfate (since we never refer to sea-salt sulfate, "sulfate" denotes "non-sea-salt sulfate" hereinafter) in these regions is gaseous dimethylsulfide (DMS) released from surface waters [*Spiro et al.*, 1992; *Bates et al.*, 1992], where it is produced by processes involving phytoplankton [*Challenger*, 1951; *Andreae*, 1986; *Nguyen et al.*, 1988]. The impacts of (1) DMS emission intensity onto CCN load and (2) changes in climatic parameters (sea surface temperature, solar flux) on phytoplanktonic activity led *Charlson et al.* [1987] to formulate the hypothesis of a possibly self-regulated climate system involving the sulfur cycle.

[3] The hypothesis of a sulfur cycle interacting with climate encourages attempts in interpreting Antarctic ice core sulfur records in terms of past climate [*Legrand and Feniet-Saigne*, 1991; *Legrand*, 1997]. However, climate affects not only intensity and location of DMS biogenic emissions, but also all the atmospheric processes involved in the sulfur cycle: transport, chemistry, deposition. Two compounds measured in ice cores, namely methanesulfonic

[1]Now at Department of Atmospheric and Oceanic Sciences, McGill University, Montreal, Quebec, Canada, and Meteorological Service of Canada, Dorval, Quebec, Canada.

0148-0227/05/2004JD004881$09.00

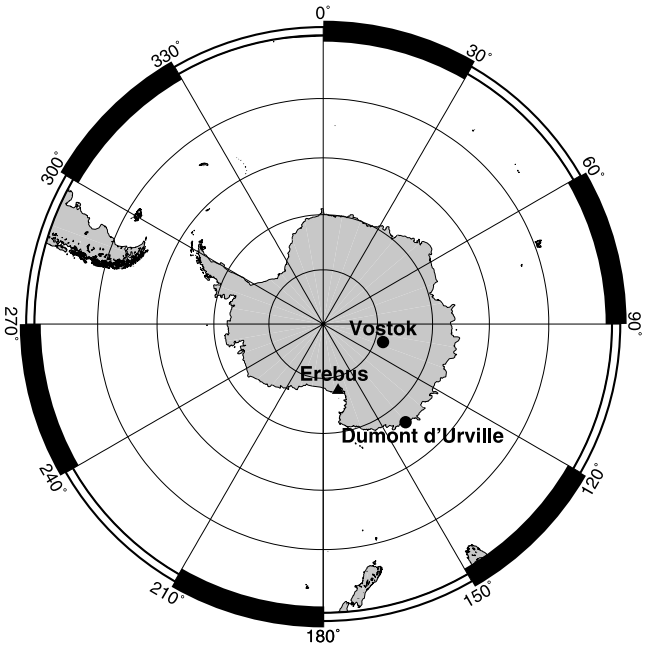

Figure 1. Location of Dumont d'Urville (140°01′E, 66°40′S) and Vostok (106°48′E, 78°28′S) research stations and of Mount Erebus, the only active volcano in the Antarctic region.

acid (MSA) and sulfate (the aerosol end-products of DMS oxidation), do not enable one to infer the implication of each of these processes. To bring solid closure hypothesis to this problem is one reason for studying the Antarctic sulfur cycle [*Berresheim and Eisele*, 1998; *Wolff et al.*, 1998].

[4] The Antarctic sulfur chemistry has been studied for several decades [e.g., *Wolff et al.*, 1998; *Berresheim and Eisele*, 1998; *Mauldin et al.*, 2001]. Significant advances has been made on its description but many aspects would deserve further attention, for instance DMS oxidation by nitrate (NO_3) radicals, especially in winter [*Koga and Tanaka*, 1996], DMS oxidation by bromine oxide (BrO) [*Toumi*, 1994], heterogeneous oxidation of dimethylsulfoxide (DMSO) by OH [*Davis et al.*, 1998; *Legrand et al.*, 2001]. Yet chemical interpretation of in situ measurements are often limited by the omnipresent role of non chemical processes, in particular emissions and transport from the source to the sites. Thus a question frequently asked by experimentalists turns toward the geographical origin of sulfur compounds [e.g., *Minikin et al.*, 1998; *Legrand and Pasteur*, 1998].

[5] Despite the numerous gaps in the knowledge of the Antarctic and sub-Antarctic sulfur cycle, some three-dimensional models appear rather successful in its representation. This is the case for instance for the GOCART model [*Chin et al.*, 2000] and the Antarctic/sulfur version of LMD-ZT [*Cosme et al.*, 2002]. Notwithstanding the defects they still display, these models are now able to provide realistic information on the origin of sulfur compounds at the Antarctic measurements stations. This is done in the present study, with LMD-ZT, for two Antarctic sites shown in Figure 1: a coastal station, Dumont d'Urville (140°01′E, 66°40′S) and an inland station, Vostok (106°48′E, 78°28′S). The former is a French scientific station used since 1991 to monitor sulfur compounds [*Minikin et al.*, 1998] and to study short-term chemical processes during intensive field campaigns [e.g., *Jourdain and Legrand*, 2001]. The latter is a Russian scientific station, well known for its 3623 m ice core [*Petit et al.*, 1999].

[6] The "standard" use of a transport model (i.e., forward in time) is clearly ill designed for interpretation of measurements at a station. A "receptor-oriented" approach based on tracer backtracking is more appropriate. The most common backtracking technique is the Lagrangian backtrajectory analysis [e.g., *Kottmeier and Fay*, 1998; *Legrand et al.*, 2001], which provides a qualitative description of the origin of air masses. A quantitative approach is possible by introducing a large enough ensemble of particles that are transported by a stochastic turbulent velocity field in addition to the mean model-resolved wind field [*Flesch et al.*, 1995; *Seibert and Frank*, 2003]. In fact, a general "retrotransport" equation can be derived that provides the time evolution of an atmospheric tracer, with possible sources and sinks, following the air trajectories backward in time. This "retrotransport" equation can be derived in a Eulerian framework as well, applying for representation of transport by unresolved turbulent or convective motions, the parametrizations usually derived for direct transport computations [*Hourdin et al.*, 1999; F. Hourdin and O. Talagrand (Eulerian backtracking of atmospheric tracers: I. Adjoint derivation and parameterization of subgrid-scale transport, submitted to *Quarterly Journal of the Royal Meteorological Society*, 2004 (hereinafter referred to as Hourdin and Talagrand, submitted manuscript, 2004)]. The retrotransport equation derived this way is also the adjoint of the direct transport equation for an air-weighted scalar product.

[7] When using retrotransport to analyze a particular measurement of a conservative tracer (in the absence of sources or sinks), the field that is transported back in time is, to a multiplying factor, the mass concentration of the air that will contribute to this measurement (for instance the distribution of the air that will be sampled later on at a station). More generally, in the presence of linear sources and sinks, the retrotracer can be interpreted as the sensitivity of the tracer concentration detected at a site with respect to any tracer input (emission, initial distribution), also called "influence function."

[8] This work makes use of retrotransport algorithms as implemented in the Eulerian global model LMD-ZT by F. Hourdin et al. (Eulerian backtracking of atmospheric tracers: II. Numerical aspects, submitted to *Quarterly Journal of the Royal Meteorological Society*, 2004) (hereinafter referred to as Hourdin et al., submitted manuscript, 2004). The retrotransport model is obtained from the direct model by very simple formal transforms (changing the direction of time and winds and inverting the role of up- and downdraughts in the mass flux parametrization of cumulus convection). For the present study, the retrotransport method is extended to account for a (linear) sulfur "retrochemistry." The direct chemistry-transport model can be described as a set of transport equations for the individual species coupled through a matrix of chemical reactions. The retrochemistry-transport model is obtained by coupling the individual retrotransport equations with the transpose of the matrix of chemical reactions. This receptor-oriented model gives directly access to the relative contributions of

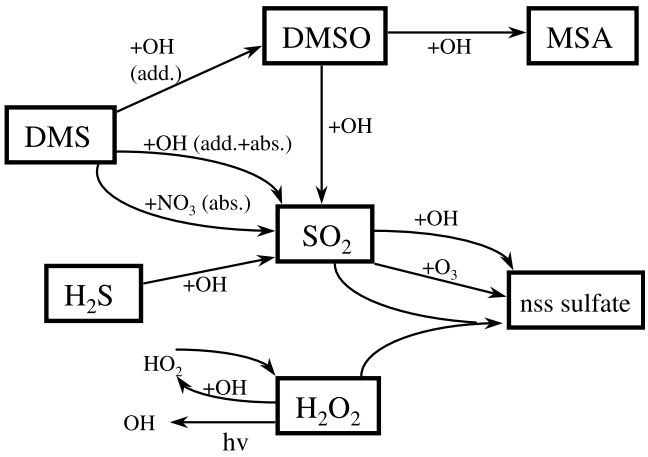

Figure 2. Chemistry scheme used in LMD-ZT. Details of the kinetics are presented by *Cosme et al.* [2002]. Here, "add." and "abs." refer to the addition and abstraction channels of DMS oxidation, respectively. SO_2 oxidation by O_3 and H_2O_2 occurs in the aqueous phase.

the different emissions to the observations of sulfur species such as those recorded in Dumont d'Urville or Vostok.

[9] The paper is organized as follows. In section 2, the model used, LMD-ZT, is introduced, with a particular emphasis on the chemistry scheme and the prescribed sulfur sources. In section 3, we merely recall the property of time symmetry of the transport equation without fully detailing the theory of retrotransport. We focus on the use we make of the retrotransport method for our purpose: to compute the sensitivity of a tracer concentration at a particular site to its emission sources, and the contribution of one source from a continuum, to the tracer concentration. Then we present how sulfur chemistry is considered in the retrotransport modeling. In section 4, we provide a detailed description of the experimental design in order to study (1) how transport and chemistry influence Dumont d'Urville (section 5) and (2) the origin of sulfur species at Dumont d'Urville and at Vostok (section 6). A summary is given in section 7.

2. Model Description

2.1. LMD-ZT GCM

[10] LMD-ZT is the Laboratoire de Météorologie Dynamique (LMD, Paris, France) general circulation model. A "zoom" ("Z") capability enables us to perform high-resolution regional studies without loosing the global coverage of the Earth: Interactions of the region of interest with the rest of the world are explicitly computed. This is a practical advantage for atmospheric chemistry studies, for it can be uneasy to define two-dimensional (2-D) boundary conditions of tracer concentrations at the borders of a regional model. The letter "T" in LMD-ZT stands for "tracers," since the model contains a tracer module. The physics of the climate part of this model are optimized for polar regions, and the grid is stretched in latitude to focus on the high southern latitudes [e.g., *Cosme et al.*, 2002]. These specificities improved the representation of Antarctic climate [*Krinner et al.*, 1997]. Sea surface temperature and sea ice cover are prescribed from satellite data, with interannual variability, and the atmospheric circulation is nudged "laterally," i.e., only at the periphery of Antarctica, to ECMWF analyses: The wind and surface pressure fields of the model are initialized to analysis values at 40, 50, and 60°S at every time step. This provides realistic variability of atmospheric circulation in the Antarctic region [*Genthon et al.*, 2002]. Tracers are transported following a finite volume transport scheme [*Van Leer*, 1977; *Hourdin and Armengaud*, 1999] for large-scale advection, and a mass flux scheme [*Tiedtke*, 1989] for convection. *Hourdin et al.* [1999] and *Hauglustaine et al.* [2004] have shown that LMD-ZT provides an efficient large-scale transport and mixing of tracers.

2.2. Sulfur Chemistry

[11] The standard sulfur version of LMD-ZT was first presented by *Boucher et al.* [2002] (available at http://www.ipsl.jussieu.fr/poles/Modelisation/NotesSciences.htm). Four sulfur gases, DMS, sulfur dioxide SO_2, hydrogen sulfide H_2S, dimethylsulfoxide DMSO, and two sulfur aerosols, sulfate and MSA, are predicted. They all undergo dry and wet deposition. The sulfur oxidation scheme is shown in Figure 2. Hydrogen peroxide (H_2O_2) is computed online. Other oxidants (hydroxyl OH, hydroperoxyl HO_2, nitrate NO_3 radicals and ozone O_3) and photodissociation rates of H_2O_2 are prescribed from the IMAGES model [*Müller and Brasseur*, 1995]. It is stressed here that because of the prescription of oxidants, gas-phase chemistry is a linear process with respect to the sulfur compounds concentrations. On the contrary, aqueous-phase chemistry is not linear. Aqueous chemistry is represented as SO_2 oxidation by O_3 and H_2O_2. The reaction rate of H_2O_2 with SO_2 is pH dependent, and the pH itself depends on sulfate concentration (see *Boucher et al.* [2002] for more details).

2.3. Sulfur Emissions

[12] Table 1 shows the global emission fluxes of sulfur species used in LMD-ZT, and the ranges of these fluxes provided by the Intergovernmental Panel on Climate Change (IPCC) [*Penner et al.*, 2001]. All our fluxes fall within the ranges of the IPCC except for volcanoes. This is because only noneruptive emissions are considered, whereas the range includes eruptive emissions.

[13] For anthropogenic sulfur emissions, we use the inventory developed in the framework of the Global Emissions Inventory Activity (GEIA) by *Benkovitz et al.* [1996]. Emissions occur mostly as SO_2, a fraction (5%) being emitted directly as sulfate. We also consider an anthropogenic source of H_2S proportional (by a factor of 0.0426) to the SO_x source as suggested by *Watts* [2000]. Volcanoes release $\sim$4.8 Tg S yr^{-1} of SO_2 [*Andres and Kasgnoc*, 1998]. One volcano, Mount Erebus, is located in the Antarctic region, at 167°25′E, 77°30′S (Figure 1). It is the only non oceanic sulfur source south of 60°S. Emissions from the biosphere and biomass burning are the same as in the IMAGES model [*Pham et al.*, 1995]. They are much smaller than anthropogenic, volcanic, and oceanic emissions. DMS emission fluxes from the ocean are computed online using the DMS seawater concentration data of *Kettle et al.* [1999] and the parameterization of *Liss and Merlivat* [1986], using the wind and surface temperature fields of LMD-ZT. This data set has been identified as the best as far

Table 1. Global Emission Fluxes of Sulfur Species in LMD-ZT[a]

Source	DMS	SO_2	Sulfate	H_2S	Total	References[b]	Range [*Penner et al.*, 2001]
Ocean	21 (5.8)				21 (5.8)	1	13–36
Anthropogenic		62.5 (0)	3.3 (0)	2.8 (0)	68.6 (0)	2, 3	60–100
Volcanoes		4.8 (0.3)			4.8 (0.3)	4	6–20
Biomass burning		3 (0)			3 (0)	5, 6	1–6
Biosphere	0.3 (0)			0.5 (0)	0.8 (0)	7, 8, 9, 10	0.4–5.6
Total	21.3 (5.7)	70.3 (0)	3.3 (0)	3.3 (0)	98.2 (1.25)		

[a]Fluxes are given in Tg S yr^{-1}. Numbers in parentheses represent the percentage emitted south of 60°S. The ranges integrate estimates from various emission inventories reported by *Penner et al.* [2001].

[b]References: 1, *Kettle et al.* [1999]; 2, *Benkovitz et al.* [1994]; 3, *Watts* [2000]; 4, *Andres and Kasgnoc* [1998]; 5, *Müller* [1992]; 6, *Delmas and Servant* [1983]; 7, *Guenther et al.* [1989]; 8, *Pham et al.* [1995]; 9, *Andreae and Andreae* [1988]; 10, *Andreae et al.* [1990].

as the middle and high latitudes are concerned [*Cosme et al.*, 2002], although they should be considered cautiously, because of the scarcity of measurements, especially in the Southern Ocean [*Kettle and Andreae*, 2000]. Sea surface temperature and sea ice extent are prescribed from GISST data of the Met Office. A lid effect of sea ice is considered [*Cosme et al.*, 2002]. The global mean annual DMS flux from ocean is about 21 Tg S yr^{-1} but varies interannually. DMS oceanic emissions approximately represent 86% of sulfur emissions south of 30°S, and 98.8% of emissions south of 60°S. Then, although oceanic DMS emissions represent only 21% of the global emissions and 71% of the natural emissions, they are expected to have a major contribution to the Antarctic sulfur cycle, as it has already been shown (but not quantified) in previous observational or modeling works [e.g., *Minikin et al.*, 1998; *Davis et al.*, 1998; *Cosme et al.*, 2002].

2.4. Evaluation of the Antarctic Sulfur Model

[14] The Antarctic sulfur version of LMD-ZT was validated using Antarctic and sub-Antarctic station data by *Cosme et al.* [2002]. It reproduces most aspects of the seasonal variations of sulfur species observed in Antarctica. This is largely due to the seasonality of oceanic DMS fluxes. Because DMS fluxes are climatological, the model fails in reproducing the interannual variability of atmospheric sulfur concentrations in spite of a realistic representation of meteorology [*Genthon et al.*, 2002].

[15] Some defects were identified. Two important ones concern DMSO formation and destruction. One leads, in particular, to underestimate MSA levels all over the year. A third important defect is that in-cloud scavenging of MSA and sulfate by polar precipitation is too strong. Impacts of these three defects on the results of this work are discussed in section 6.4. Another potential drawback comes from the prescribed concentrations of OH: At the South Pole in summer, in situ measurements [*Mauldin et al.*, 2001] showed OH levels 10 times higher than the levels prescribed in the model. This was found to be of minor importance, as most of sulfate and MSA precursors are present in very low concentrations and do not induce sulfate and MSA formation. Thus this defect is not discussed in what follows.

[16] The version used in the present work differs from that of *Cosme et al.* [2002] by only one feature: Here, the oceanic DMS fluxes are computed online instead of using the off-line-computed flux fields of *Kettle et al.* [1999]. This change does not deteriorate nor significantly improve the mean sulfur cycle representation [*Cosme*, 2002], but it enhances interannual variations.

3. Retrotransport of Tracers

3.1. Time Symmetry of Transport Equation for a Passive Tracer

[17] Let us note ρ the atmospheric air density (in kg m^{-3}), Ω the space domain (the atmosphere), and τ a time interval. The time symmetry of transport equation described by *Hourdin and Issartel* [2000] is embodied by equation (6) of Hourdin and Talagrand (submitted manuscript, 2004):

$$\int_{\Omega\times\tau} \rho\sigma^* c\,\mathbf{dx}dt = \int_{\Omega\times\tau} \rho\sigma c^*\,\mathbf{dx}dt \tag{1}$$

provided c (tracer concentration, in molecules kg^{-1} of air) obeys the atmospheric transport equation with the source term σ,

$$Lc = \sigma, \qquad L = \partial/\partial t + \mathbf{u}.\mathbf{grad} + C(.) - \frac{1}{\rho}\frac{\partial}{\partial z}\left(\rho k \frac{\partial}{\partial z}\right) + \lambda, \tag{2}$$

and c^* is solution of the "retrotransport" equation with the source term σ^*

$$L^*c^* = \sigma^*, \quad L^* = -\partial/\partial t - \mathbf{u}.\mathbf{grad} + C^*(.) - \frac{1}{\rho}\frac{\partial}{\partial z}\left(\rho k \frac{\partial}{\partial z}\right) + \lambda. \tag{3}$$

Here, **u** is the large-scale air mass velocity, and **u.grad** is the corresponding advection term. $C(.)$ represents a mass flux parameterization of convective transport. $-(1/\rho)\ (\partial/\partial z)\ [\rho k(\partial c/\partial z)]$ is a parameterization of the turbulent mixing, considered only in the vertical dimension. k is a diffusion coefficient (in $m^2\ s^{-1}$). λ is a multiplying (possibly varying in space and time) scalar that gathers the effects of dry and wet deposition, and radioactive decay if it exists. There is no chemistry here.

[18] Turbulent diffusion, aimed to parameterize the mixing by symmetric upward and downward motions, is unchanged in the retrotransport equation. Decay (λ) also remains unchanged. For the parameterization of unsymmetric convective transport (operator C) we use in the direct model the mass flux algorithm developed by *Tiedtke* [1989], which explicitly divides the atmospheric column between concentrated convective updraughts, rapid downdraughts

associated to rainfall and compensatory subsidence in the environment. In the retrotransport mode (operator C^*), the vertical air fluxes and exchanges between those compartments are just reversed [*Hourdin and Issartel*, 2000; Hourdin and Talagrand, submitted manuscript, 2004].

[19] Equation (1) means that L and L^* are adjoint following the inner product

$$\langle f, g\rangle = \int_{\Omega\times\tau} \rho f g \mathbf{dx} dt, \tag{4}$$

where f and g belong to the space $L^2(\Omega \times \tau)$ of the real functions integrable with square in the domain $\Omega \times \tau$. L^* has been derived on pure physical considerations by *Hourdin and Issartel* [2000], but it can also be retrieved from equation (1) through integrations by parts of the right hand side integral.

[20] In practice with a GCM, equation (2) is integrated by simultaneously computing meteorology. Equation (3) cannot, since it uses the "real" meteorological variables, and not an inversed meteorology. Then the model is first run forward, calculating dynamical and physical variables of the atmospheric circulation, and the evolution of tracer concentrations. During this simulation, parameters needed for the tracer processing (air mass fluxes for large-scale and convective advections, cloudiness and precipitating water fluxes for scavenging, and parameters for the boundary layer mixing) are averaged and archived with a 6 hour time step. Equation (3) is then solved using these data backward in time, inversing large-scale and convective transport processes, but maintaining the other processes in forward-like mode.

[21] The retrotransport model is obtained from the direct model by only changing some signs in the transport equation. Thus the accuracy of the retrotransport model is exactly the accuracy of the direct model. Limitations of the retrotransport approach arise when the time symmetry is broken. This occur when nonlinearities are introduced in the model, such as chemistry.

3.2. Retrotransport and Sensitivities

[22] To intuitively introduce how the retrotransport is used for our purpose, let assume that in the "real" space (in which the evolution of tracer concentration is driven by operator L) a quantity Q_s of tracer is released at a source site S, at time t_s, considered as a point source in space and time (the atmosphere is assumed to be free of tracer before t_s). We note $c(D, t_d)$ the tracer concentration detected at a detection site D and at time t_d ($t_d > t_s$), after L had operated. Analogously, we note Q_d^* a quantity of tracer released at the site D and time t_d in the "adjoint" space (the atmosphere being free of adjoint tracer for $t > t_d$), in which the backward evolution of tracer concentration is driven by the operator L^*, and $c^*(S, t_s)$ the corresponding tracer concentration measured at S and time t_s. We assume here that the atmosphere is a closed medium (no exchange of tracer with outside).

[23] Then tracer concentrations c and c^* follow the equations

$$Lc = \delta(S, t_s).Q_s, \tag{5}$$

$$L^*c^* = \delta(D, t_d).Q_d^*, \tag{6}$$

respectively, where δ is the Dirac function: $\delta(M, t_m)$ is equal to 1 at the location M, time t_m, and 0 elsewhere in space and time. The combination of equations (1), (5), and (6) leads to the following relation between the source term and the detector term:

$$\rho(S, t_s).c^*(S, t_s).Q_s = \rho(D, t_d).c(D, t_d).Q_d^*. \tag{7}$$

The physical meaning of $c^*(S, t_s)$ can be grasped by writing the differentiate form of equation (7) with fixed adjoint quantities (Q_d^* and $c^*(S, t_s)$):

$$\frac{\delta c(D, t_d)}{\delta Q_s} = \frac{\rho(S, t_s)}{\rho(D, t_d)} \frac{c^*(S, t_s)}{Q_d^*}. \tag{8}$$

In this form, the right-hand-side term of equation (8) appears to be the sensitivity of the tracer concentration $c(D, t_d)$ to intensity of the source S at t_s. In other terms, a small perturbation δQ_s of S intensity at t_s brings about a perturbation of $(\rho(S, t_s)/\rho(D, t_d))(c^*(S, t_s)/Q_d^*)\delta Q_s$ in the concentration $c(D, t_d)$.

3.3. Contribution of Sources to the Measurement

[24] Section 3.2 presented a calculation of the sensitivity of a tracer concentration to intensity of a point source.

[25] More generally, the tracer concentration c driven by equation (2) depends on (1) the tracer field at initial time t_i, (2) the inflow of tracer into the system (equal to zero for our global model) and (3) the sources term σ. When the tracer is emitted at the surface, the source σ_s (in molecules m^{-2} s^{-1}) is rather described as a boundary condition for vertical turbulent diffusion. For the retrotransport, it is theoretically equivalent to an explicit surface emission flux (Hourdin and Talagrand, submitted manuscript, 2004).

[26] Using the adjoint model with a quantity Q_d^* of tracer released at D, time t_d, with an adjoint tracer equal to zero for $t > t_d$, with no emission at the surface ($\sigma_s^* = 0$), the spatiotemporal field c^* issued from 6 allows us to rewrite the concentration in D at t_d as the sum of contributions from initial conditions and sources as

$$\rho(D, t_d).c(D, t_d).Q_d^* = \int_\Omega \rho(\mathbf{x}, t_i) c^*(\mathbf{x}, t_i) \sigma(\mathbf{x}, t_i) \mathbf{dx} \tag{9}$$

$$+ \int_{\Omega\times\tau} \rho(\mathbf{x}, t) c^*(\mathbf{x}, t) \sigma(\mathbf{x}, t) \mathbf{dx} dt + \int_{\Omega_s\times\tau} c^*(\mathbf{x}_s, t) \sigma_s(\mathbf{x}_s, t) \mathbf{dx}_s dt \tag{10}$$

where Ω_s is the surface, σ_s is the surface emission flux (in molecules m^{-2} s^{-1}), and $\mathbf{dx}_s$ is a surface element (m^{-2}) at the surface location $\mathbf{x}_s$.

[27] For a tracer with a finite life time ($\lambda > 0$), the contribution of the initial concentration decreases as the time lag between initial time t_i and detection t_d increases. For a long enough time interval, and if the tracer is emitted at the surface only ($\sigma = 0$), the measurement finally reads

$$\rho(D, t_d).c(D, t_d).Q_d^* = \int_{\Omega_s\times\tau} c^*(\mathbf{x}_s, t) \sigma_s(\mathbf{x}_s, t) \mathbf{dx}_s dt \tag{11}$$

or, in a discrete form,

$$\rho(D,t_d).c(D,t_d).Q_d^* = \sum_{t_j\in\tau}\sum_{\mathbf{x}_i\in\Omega_s} c^*(\mathbf{x}_i,t_j)\sigma_s(\mathbf{x}_i,t_j)\Delta\mathbf{x}_s(\mathbf{x}_i)\Delta t, \tag{12}$$

where Δt is the discrete time step (in seconds) and $\Delta\mathbf{x}_s$ is the bottom surface of the grid point (m^{-2}). Here Ω_s describes the first model layer. So we see that the emission of tracer at grid point l contributed

$$100\times\frac{c^*(\mathbf{x}_l,t_k).\sigma_s(\mathbf{x}_l,t_k)\Delta\mathbf{x}_s(\mathbf{x}_l)\Delta t}{\rho(D,t_d).c(D,t_d).Q_d^*}\ \% \tag{13}$$

to the measured concentration $c(D, t_d)$.

3.4. Extension to Chemically Active Sulfur Tracers

[28] Chemistry introduces possibly nonlinear relations between different tracers. However, as far as the real atmospheric sulfur cycle in the middle and high southern latitudes (and over most of the globe, actually) is concerned, sulfur chemistry can be quite accurately approximated with a linear chemistry module. This is the case for the gas phase in our model, as is often the case in general circulation models imbedding only sulfur chemistry. The concentrations of the main oxidants of sulfur compounds (OH and NO_3 radicals) are prescribed, either because the variations of sulfur species concentrations weakly affect their concentrations or because they depend on mechanisms for which modeling is too complex and CPU consuming to be considered advantageous in the context of a global sulfur cycle study.

[29] In the presence of several tracers, the system evolution is described by the set of the transport equations of each tracer. We consider for simplicity a system of two species A and B, A reacting with OH of fixed (prescribed) concentration to form B, with a rate K. Then a loss term for A (K[OH][A]) and a production term for B ($-K$[OH][A]) complete the left-hand sides of the evolution equations (equation (2)) of A and B, respectively. These two equations can be gathered together in matrix form:

$$\begin{pmatrix} L_A+K[\mathrm{OH}] & 0 \\ -K[\mathrm{OH}] & L_B \end{pmatrix}\begin{pmatrix}[A]\\ [B]\end{pmatrix} = \begin{pmatrix}\sigma_A\\ \sigma_B\end{pmatrix}, \tag{14}$$

where $L_A = \partial/\partial t + \mathbf{u}.\mathbf{grad} + C(.) - 1\rho(\partial/\partial z)[\rho k(\partial/\partial z)] + \lambda_A$ and $L_B = \partial/\partial t + \mathbf{u}.\mathbf{grad} + C(.) - (1/\rho)(\partial/\partial z)[\rho k(\partial/\partial z)] + \lambda_B$. Similarly to the other parameters (effects of deposition, convection, and turbulent mixing), the term K[OH] can be archived during the forward simulation. The square matrix in equation (14) defines a linear operator on $[L^2(\Omega\times\tau)]^2$. Analogously to the case of the passive tracer, the space $[L^2(\Omega\times\tau)]^2$ can be equipped with the inner product F defined as

$$F(f,g) = \langle f_1,g_1\rangle + \langle f_2,g_2\rangle, \tag{15}$$

where $\langle .,.\rangle$ is the inner product on $L^2(\Omega\times R)$ defined in equation (4) and $f = (f_1, f_2)$ and $g = (g_1, g_2)$ are two functions of $[L^2(\Omega\times R)]^2$. L has an adjoint L^* following the inner product F:

$$L^* = \begin{pmatrix} L_A^*+K[\mathrm{OH}] & -K[\mathrm{OH}] \\ 0 & L_B^* \end{pmatrix}, \tag{16}$$

where L_A^* and L_B^* are the respective adjoints of L_A and L_B. They are similar to the adjoints defined without chemistry. The system solved by the retrotransport model is then

$$\begin{pmatrix} L_A^*+K[\mathrm{OH}] & -K[\mathrm{OH}] \\ 0 & L_B^* \end{pmatrix}\begin{pmatrix}[A]^*\\ [B]^*\end{pmatrix} = \begin{pmatrix}\sigma_A^*\\ \sigma_B^*\end{pmatrix}, \tag{17}$$

where $[A]^*$, $[B]^*$ are the concentrations, and σ_A^*, σ_B^* the sources intensity in the adjoint space.

[30] Let us assume that B is only formed by the reaction of A with OH, not emitted ($\sigma_B = 0$), and that a quantity Q_A of A is released at position S, at time t_s ($\sigma_A = \delta(S, t_s).Q_A$). Concentrations $[A]$ and $[B]$ are driven by equation (14), and at position D, and time t_d, a concentration $[B](D, t_d)$ is simulated. This stands for the real space. We now consider the adjoint space, where concentrations $[A]^*$ and $[B]^*$ evolve under the effect of operator L^* (equation (17)). There is no source of A ($\sigma_A^* = 0$) but there is a source of B at position D and time t_d ($\sigma_B^* = \delta(D, t_d).Q_B^*$). Noting $c = ([A], [B])^T$ and $c^* = ([A]^*, [B]^*)^T$, we obtain

$$F(Lc,c^*) = Q_A.\rho(S,t_s).[A]^*(S,t_s), \tag{18}$$

$$F(c,L^*c^*) = Q_B^*.\rho(D,t_d).[B](D,t_d) \tag{19}$$

and, eventually,

$$\rho(S,t_s).[A]^*(S,t_s).Q_A = \rho(D,t_d).[B](D,t_d).Q_B^*. \tag{20}$$

Equation (20) is analogous to equation (7) but for two species linked by a chemical reaction. $[A]^*(S, t_s)/Q_B^*$ is then the sensitivity of the tracer concentration $[B](D, t_d)$ to intensity of the source (of species A) S at t_s, in a given atmospheric chemical state. If A is emitted by a source continuum instead of a point source, one can convolve the previously computed sensitivity with the A source, as presented in section 3.3, to get the contribution of each source of A to the amount of B detected at the detector D, at time t_d. It is also possible to compute the contribution of each source of A to the amount of A (which has not been oxidized) itself.

[31] Of course these considerations can be extended to any number of species and oxidants (in our model there are 6 species and 2 oxidants for gas-phase chemistry) provided chemistry is linear.

[32] As presented in section 2.2, aqueous chemistry introduces nonlinearities in the evolution equation of SO_2 and sulfate. H_2O_2 concentrations are computed online and therefore are affected by SO_2 concentrations. Thus SO_2 concentrations at a given time are affected by SO_2 concentrations in the past. Moreover, the rate of their reaction

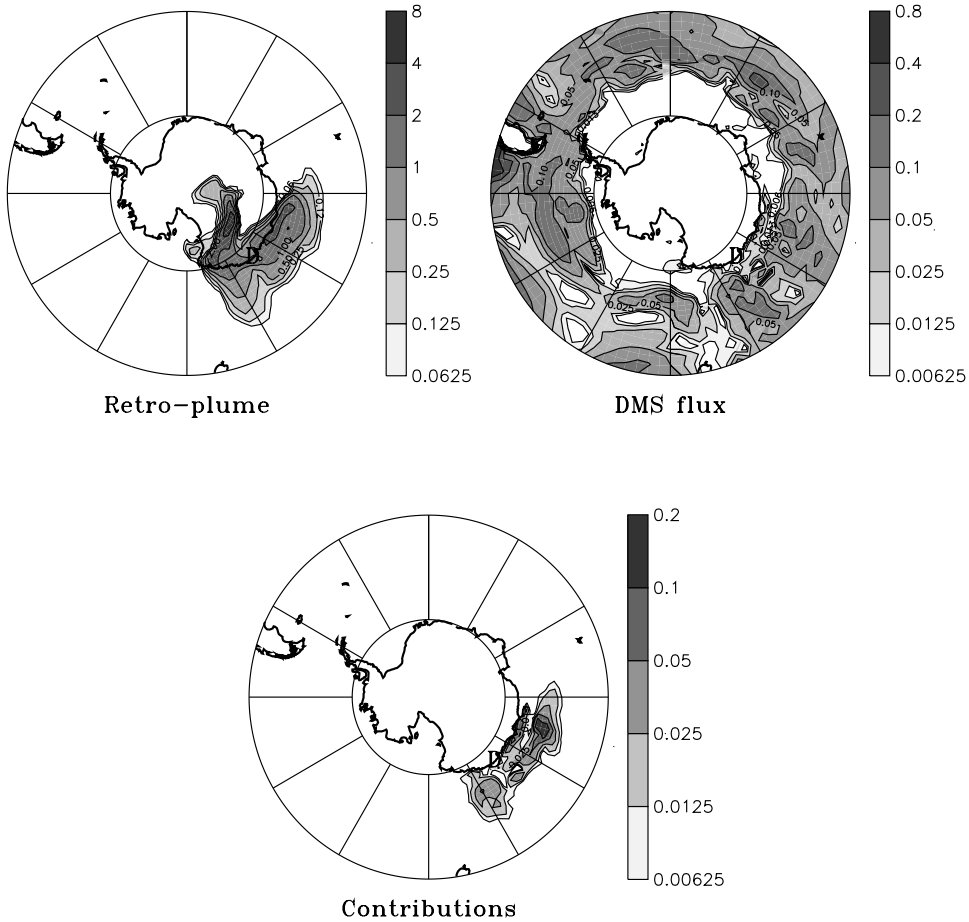

Figure 3. Retroplume of DMS in the first model layer on 27 July 1999, generated by a release of sulfate at Dumont d'Urville on 30 July (units: molecules per 10 km^3) (upper left map); oceanic DMS flux on 27 July (units: mg sulfur m^{-2} d^{-1}) (upper right map); contributions of DMS sources of 27 July to sulfate at Dumont d'Urville on 30 July (units are percent per 100 km^2) (bottom map). Dumont d'Urville is indicated by "D." See color version of this figure at back of this issue.

depends on SO_2 and sulfate concentrations through the pH. These non linear effects prevent from directly defining the adjoint of the chemistry-transport model. In this case, frequently encountered in adjoint methods, the standard solution is to derive the tangent linear model first, then its adjoint. However, it would have considerably complexified the concept of contribution as defined in the previous section. Instead, we consider the rate of SO_2 oxidation in aqueous phase as known and independent of sulfur concentrations. In practice, the rate of SO_2 to sulfate conversion in aqueous phase is stored during the forward runs. This rate is analogous to K[OH] considered previously for the gas phase chemistry. In a very unfavorable case (with high nebulosity and in summer, when H_2O_2 concentrations are high), this approach generates errors below 25%. This simplified approach, albeit not theoretically rigorous, provides a good approximation of aqueous chemistry and enables one the definition of sources contributions.

4. Experiment Design

[33] The method of retrotransport is applied to address the origin of sulfur compounds at Dumont d'Urville (coastal Antarctica, see Figure 1) and Vostok (inland Antarctica), in January (representing summertime) and July (wintertime).

4.1. Simulations and Computation of "Retroplumes"

[34] The model is first run forward (i.e., following the tracer transport equation (2), completed with chemical production and loss terms) for 5 years (1995–1999), archiving the necessary data for the months of January, June and July. Then it is run backward (i.e., following equation (3), including chemistry) 16 times: for both sites, with a release of four tracers (DMS, sulfate, MSA and DMSO) on 30 January and 30 July. For January, the model is run over one month. We verified that emissions older than one month have a negligible contribution. This is not the case in winter, because of slower chemistry than in summer; thus the model is run backward over July and June.

[35] The retrotransport simulations generate sensitivity fields or "retroplumes." Figure 3, upper left, shows an example of a retroplume. It is a polar projection of the retroplume of DMS 3 days after the sulfate release at Dumont d'Urville on 30 July 1999. The units (not important

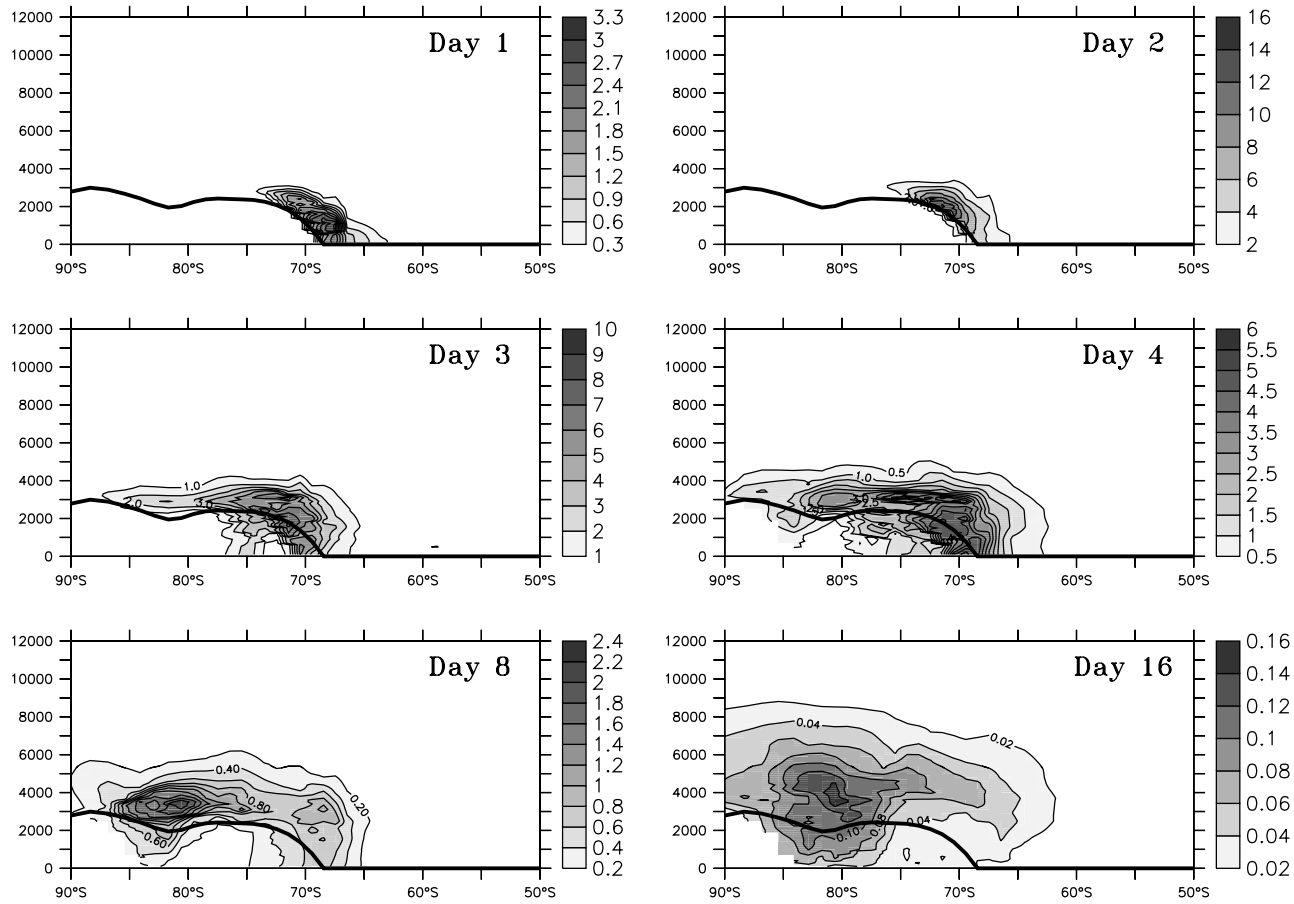

Figure 4. Vertical section (maximum values along the longitudes) of the 5-year mean retroplume of DMS generated by a release of sulfate at Dumont d'Urville (located on the coast, at 66°40′S) in January. Units are molecules per 10 km^3 volume, with 86,400 molecules having been released. "Day 1" refers to the day of release, "day 2" refers to the day before, and so on. The thick line roughly reproduces the minimal altitude of the ice cap between 130° and 150°E, where the coastal station is located. See color version of this figure at back of this issue.

for the present discussion) are molecules per 10 km^3 volume of air. A total of 86,400 molecules were released at a constant rate (1 per second) during one day.

[36] The retroplume maximum (the highest sensitivity) is found inside the continent. This means that if a DMS source was present there, it would greatly contribute to the sulfate load at Dumont d'Urville 3 days after. However, it does not mean that sulfate at Dumont d'Urville comes from this location, nor that DMS has been oxidized at this location. Only the combination of the retroplumes with the source fields provides information about the real origin of sulfate. The combination of the retroplume of Figure 3 with the oceanic DMS sources of the same day (Figure 3, upper right) is shown in Figure 3, bottom. Because there is no DMS source on the continent, there is no contribution from the continent. Also, for instance, because the retroplume has negligible values near the Antarctic peninsula, there is no contribution from this region, even if there are sources.

[37] Some retroplumes are analyzed directly for Dumont d'Urville, in section 5. This allows us to assess how transport (section 5.1) and chemistry (section 5.2) affect the coastal station.

4.2. Computation of Source Contributions

[38] As illustrated previously through Figure 3, retroplumes were convolved with emission fluxes to get the spatiotemporal (and by type of source) distribution of contribution of each source to the four chemical species simulated on 30 January and 30 July at Dumont d'Urville and Vostok (expression (13)). Integration of these distributions over space and time (expression (12)) leads to the contributions by type of source. This is interesting only for sulfate, since it is the only compound considered here that can be produced from several sources (mainly oceanic, volcanic, and anthropogenic). The other compounds (MSA, DMSO) are exclusively oxidation products of DMS. The contribution of each type of source to sulfate is addressed in section 6.1. Integration over the types of sources, time and longitude leads to the meridional distribution of sources. The location of the biogenic emissions of DMS that produced the four species is presented in

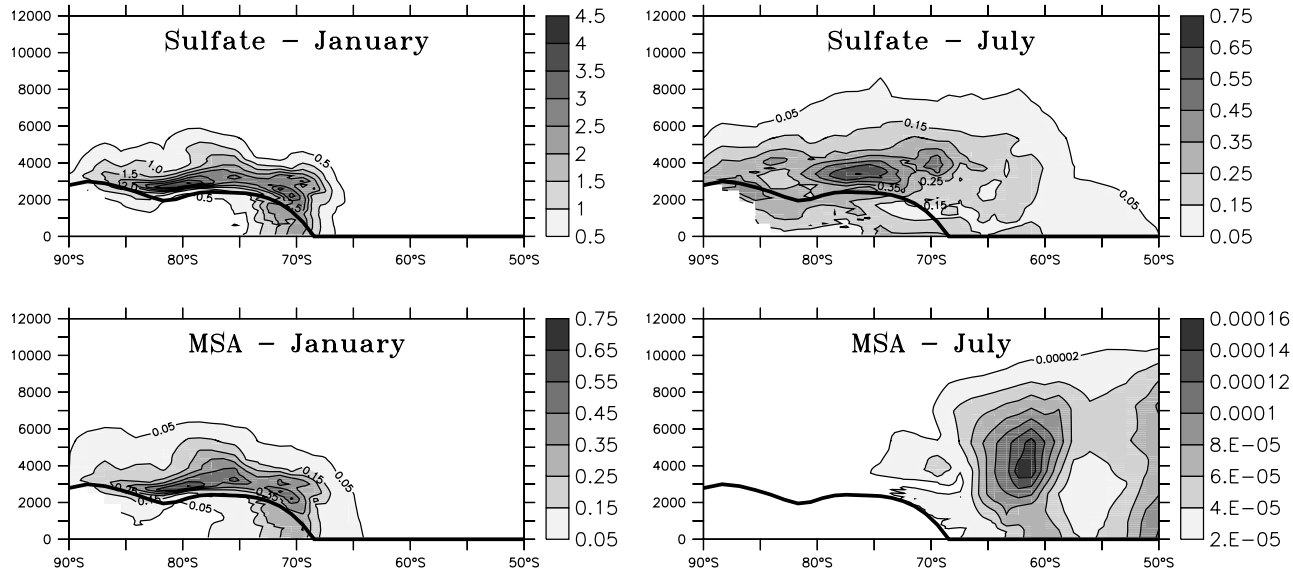

Figure 5. Vertical sections (maximum values along the longitudes) of the 5-year mean retroplumes of DMS, 5 days after releasing sulfate (upper panels) or MSA (lower panels), in (left) January or (right) July, at Dumont d'Urville. See color version of this figure at back of this issue.

section 6.2. Integration over the types of sources and space (longitude, latitude), leads to the contribution of each day preceding sulfate detection. Weighting each day with its own contribution allows us to compute the mean age of sulfur species at Dumont d'Urville and Vostok. "Age of sulfur species" must be understood as the time since the emissions that led to the formation of the species took place, and not the time since the formation of the species took place, i.e., through the oxidation of another species. The mean ages of DMS, sulfate and MSA are addressed in section 6.3. In section 6.4, we finally address how known model defects may influence these results.

5. How Do Transport and Chemistry Influence Dumont d'Urville?

5.1. Transport

[39] Figure 4 shows a vertical section of the 5-year mean retroplume of DMS generated by a release of sulfate at Dumont d'Urville on 30 January. To better backtrack the retroplume core using a vertical section representation, the maximum value along each longitude is taken, for each latitude and altitude. On the day of the release and the three previous days, the retroplume is taken by the (retro-) katabatic winds toward the interior of the continent. In Adélie Land, the Antarctic sector where Dumont d'Urville is located, it is indeed well known that surface winds are largely dominated by the katabatic effects [*König-Langlo et al.*, 1998]. The katabatic winds are initiated by a horizontal density gradient due to a slope between the cold air near the surface and the relatively warmer upper air. They are the dynamical drivers of the Antarctic atmospheric circulation [e.g., *King and Turner*, 1997]. Figure 4 suggests that they also play a major role in the distribution of the average-lived chemical species and aerosols such as sulfur compounds.

[40] After a few days, the retroplume core reaches ~80°S and remains approximately at this position several days, as illustrated by days 8 and 16. The slow rising of the retroplume during the same days is consistent with the continuous presence of a large-scale subsidence over the ice cap that balances the air mass divergence associated with the katabatic flows. The corresponding vertical velocity, of the order of 350 m d^{-1} in July and 90 m d^{-1} in January, is compatible with the available but indirect estimate of 260 m d^{-1} in winter given by *White and Bryson* [1967]. Thus transport makes Dumont d'Urville highly sensitive to hypothetical DMS sources that would be on the ice cap, upstream the station. Obviously, such sources do not exist. This is why, in spite of its poor sensitivity to the DMS emissions from the ocean (the concentrations in the retroplume in Figure 4 above the water surface are much lower than those above the continent, so that they are, most of the time, below the first units of the color scales), Dumont d'Urville is essentially under oceanic influence, as will be shown in section 6.1.

5.2. Chemistry

[41] Figure 5 shows vertical sections of the 5-year mean retroplumes of DMS, 5 days after releases of sulfate and MSA at Dumont d'Urville on 30 January and 30 July. In summer, the retroplumes display similar patterns, meaning that DMS is retroformed at similar kinetics whether it comes from sulfate or MSA. In winter, they are significantly different, meaning sulfate and MSA undergo distinct retro-oxidation pathways. This is a direct consequence of the (forward) chemistry involved in DMS oxidation (see Figure 2). DMS can be oxidized by OH or NO_3 radicals. The major source of OH is the reaction between H_2O and oxygen atom O^1D, formed by O_3 photolysis at solar wavelengths shorter than 310 nm. NO_3 is formed by the reaction of O_3 and NO_2 but rapidly undergo photolysis during day time. Photolysis is the main sink of NO_3 radicals. Sunlight appears then propitious to OH formation and NO_3 destruction, and its absence prevents both OH formation and NO_3

Table 2. Five-Year Mean Contributions of Each Type of Source to the Sulfate Simulated at Dumont d'Urville and Vostok, in Summer and in Winter[a]

	Dumont d'Urville		Vostok	
	Summer	Winter	Summer	Winter
Ocean (DMS)	98.9 (97–99.8)	91.2 (81.8–98.4)	97.5 (95.1–99.2)	92.4 (88.0–94.1)
Volcanoes (SO_2)	0.9 (0.1–2.8)	3.6 (0.8–14.7)	2 (0–4.6)	2.1 (0.6–6.4)
Anthropogenic (SO_x)	0.2 (0–0.6)	3.8 (0.5–8.3)	0.4 (0.2–0.6)	3.9 (3.1–4.2)
Other	~0	1.4 (0.3–2.7)	~0.1	1.6 (1–1.9)

[a]Contributions are given in percent. Numbers in parentheses represent the minimum and maximum values among the 5 years considered (1995–1999).

photolysis. As a consequence, in summer, the main DMS oxidation channel is reaction with OH radicals, and oxidation by NO_3 is negligible. DMS + OH reaction indirectly leads to both MSA and sulfate formation, with different rates but close kinetics. In a sense, after DMS is released, MSA and sulfate are produced simultaneously (in summer). In the retrotransport approach, MSA and sulfate are retro-oxidized into DMS simultaneously. The result from Figure 5 means

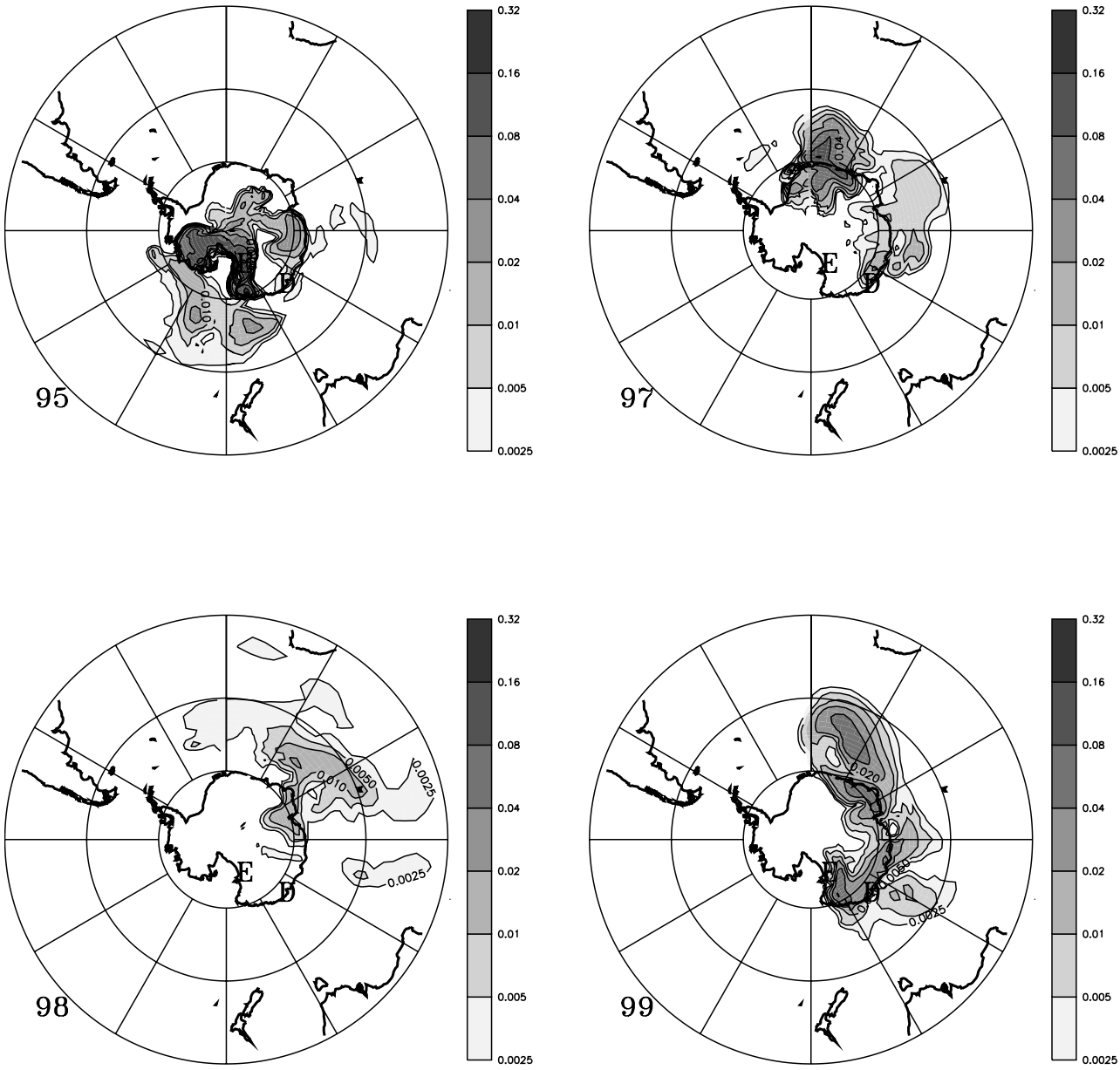

Figure 6. Retroplumes of SO_2 (in the first model layer), 3 days after a release of sulfate at Dumont d'Urville in July, for the years 1995 and 1997–1999. Dumont d'Urville is indicated by "D," and Mount Erebus is indicated by "E." See color version of this figure at back of this issue.

that in summer, both sulfate and MSA at Dumont d'Urville would be especially sensitive to a DMS source on the continent, if one existed.

[42] On the contrary, in winter, at high latitudes during the polar night, DMS oxidation is dominated by the reaction with NO_3 radicals [e.g., *Koga and Tanaka*, 1996; *Cosme et al.*, 2002], and SO_2 oxidation is dominated by aqueous reaction with O_3, so that sulfate production remains possible. MSA production, for which the presence of OH is needed in the model chemistry, is stopped inside the continent. Consequently, sulfate at Dumont d'Urville would be sensitive to a hypothetical DMS source on the continent, whereas MSA would not. Only the MSA retroplume that is not taken by the katabatic winds, and is thus able to reach lower latitudes, is retro-oxidized. Thus MSA is only sensitive to DMS sources north of ~70°S.

[43] Finally, even if sulfate production still takes place in winter, it is slower than in summer. This results in a more extended and diluted DMS retroplume in winter. In summer, the fast (retro-) chemistry results in a rather local retroproduction of DMS, then in higher DMS concentrations. This summer/winter difference may be enhanced by the more intense atmospheric circulation in winter. Thus, for sulfate too, Dumont d'Urville may be more sensitive to remote (northern) DMS sources in winter than in summer.

6. Origin of Sulfur Compounds at Dumont d'Urville and Vostok

[44] As stated above, the retroplume gives access to contributions of the sources only after combination with actual sources, what is done in this section.

6.1. Contribution of Each Type of Source to Sulfate

[45] Table 2 presents the contribution of each source to sulfate by site and season. DMS from the ocean clearly dominates, since it always provides more than 90% of sulfate at both sites and both seasons. This dominance is more pronounced in summer (98.9 and 97.5% at Dumont d'Urville and Vostok, respectively). Surprisingly, although it is farther from the midlatitudes than Dumont d'Urville, Vostok is slightly more affected than Dumont d'Urville by other sources in summer. The contributions of remote anthropogenic and volcanic sources are twice as high at Vostok. The compounds released by those remote sources (and their oxidation products) may undergo the "standard" transport scheme from middle latitudes toward Antarctica: entrainment to the middle troposphere, followed by a large-scale advection toward high latitudes, and subsidence over the Antarctic continent [*James*, 1989]. Once in the lower levels of the Antarctic atmosphere, the compounds are entrained by katabatic winds toward the coast, as seen in the previous section. During this transport, sulfate can be deposited on snow. The air arriving at the coast is thus impoverished in anthropogenic and volcanic sulfate. Whereas this process is hardly discernible in the direct simulation, in which the tracers originate from different sources and are efficiently mixed in the atmosphere during large-scale transport, the retroplume (Figure 4) illustrates it very well. This result reveals that inland Antarctica might not be less polluted than coastal Antarctica, relatively speaking (in percent of total sulfur, not in absolute).

[46] In winter, DMS contribution to sulfate still dominates, but to a lesser extent than in summer (91.2 and 92.4%). This should be primarily linked to seasonal variations of intensity of oceanic DMS source. In winter, the lower solar insolation and the presence of sea ice at high latitudes tend to reduce phytoplanktonic activity, and therefore oceanic DMS sources. Both sites, Dumont d'Urville in particular, are affected by the removal of these local DMS sources. Moreover, the circumpolar atmospheric circulation intensifies in winter. Wintertime is then propitious to large-scale tropospheric advection from middle latitudes toward Antarctica [*Krinner and Genthon*, 2003]. Note that the maximum contribution of volcanoes to sulfate at Dumont d'Urville in winter is close to 15% (for year 1995), whereas it hardly reaches 1% the other years. This high figure is due to a fast advection of air from the Ross sector, where Mount Erebus is located (Figure 1), and this is illustrated in Figure 6. This figure shows polar projections of the retroplumes of SO_2 3 days after the sulfate releases at Dumont d'Urville on 30 July in 1995 and 1997–1999. In 1995, the plume passes exactly over the volcano, whereas it goes around the other years. This example clearly reflects that, even sporadically, sources other than the oceanic DMS can affect significantly the amount of sulfate at Dumont d'Urville.

6.2. Meridional Distribution of Biogenic DMS Sources

[47] The contributions of DMS oceanic sources to DMS concentration at Dumont d'Urville, split by latitude bands of 5°, are shown in Figure 7 for summer and winter. In summer, the band 65°–70°S provides the highest mean contribution (~38%). Most of DMS (76%) comes from sources located south of 60°S. In winter, the higher contribution arises from the band 55°–60°S. The region south of 60°S contributes to only 32% of the DMS at Dumont d'Urville. These results are consistent with a reduction of biological activity in winter and the presence of sea ice at high latitudes. The longer lifetime of DMS due to reduced oxidation by OH in winter also contributes to a more distant origin of DMS in July.

[48] Figure 8 shows the meridional distribution of oceanic DMS sources contributing to MSA and sulfate at Dumont d'Urville, in summer and in winter. The distributions of MSA and sulfate sources are similar in summer. Most of the MSA and sulfate observed at Dumont d'Urville originates from DMS emitted in the 55°–70S° region (62.5% for MSA, 63.5% for sulfate). Nevertheless, in winter, the distributions for MSA and sulfate strongly differ. The contributions for sulfate are similar to those for DMS in winter (Figure 7). On the contrary, MSA originates from emissions that take place farther away from Dumont d'Urville. The highest contribution is found in the band 35°–40°S (17%). This can be attributed to the DMS oxidation scheme, as already discussed in section 5.2. In summer, because DMS is mainly oxidized by OH, the same DMS sources contribute to both sulfate and MSA simultaneously. In winter, MSA is not formed at high latitudes whereas sulfate is. This explains why they have different meridional origin, and the relatively high sulfate and low MSA concentrations observed in winter at Dumont d'Urville [*Minikin et al.*, 1998; *Jourdain and Legrand*, 2001]. Table 3 (mainly discussed in section 6.3) shows

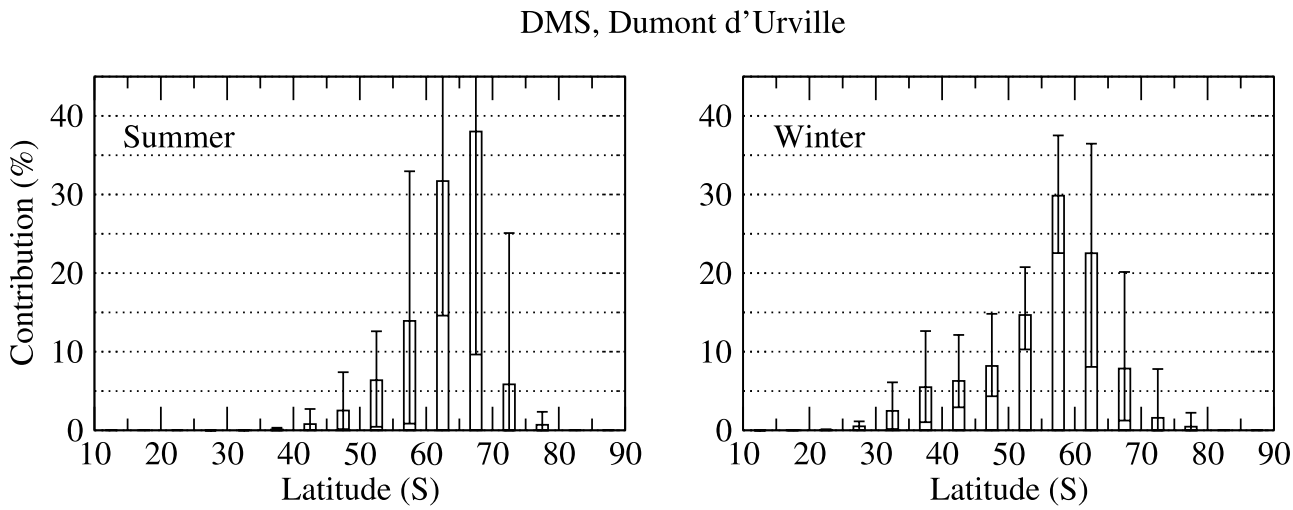

Figure 7. Meridional distribution, by 5° latitude bands, of the 5-year mean contributions of oceanic DMS sources to DMS concentration at Dumont d'Urville, in summer and in winter. Error bars indicate minimum and maximum values among the 5 years.

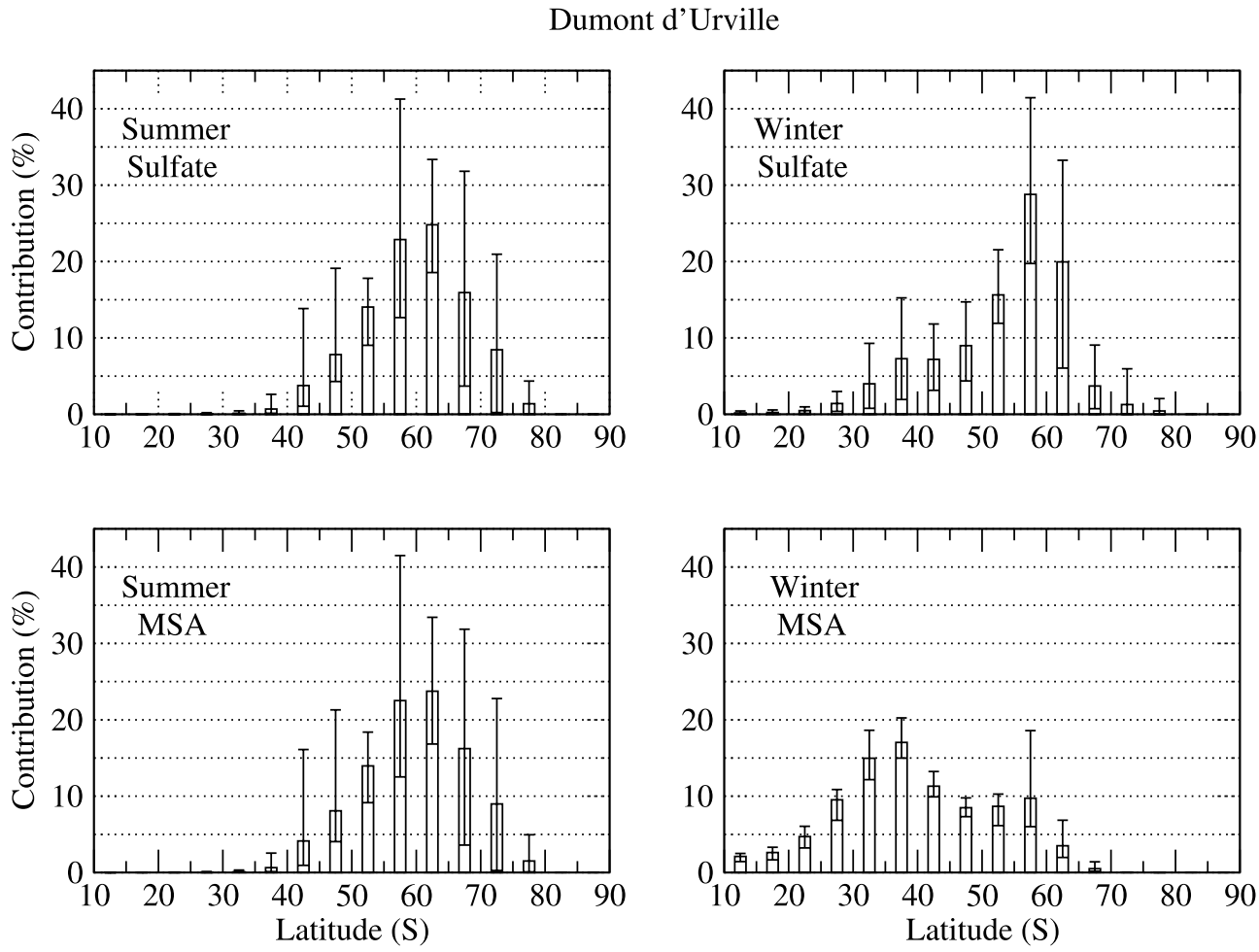

Figure 8. Meridional distribution of the 5-year mean contributions of oceanic DMS sources to sulfate and MSA concentrations at Dumont d'Urville, in summer and in winter. Error bars indicate minimum and maximum values among the 5 years.

Table 3. Five-Year Mean Chemical Lifetimes of DMS and Ages of DMS, Sulfate, MSA, and MSA + DMSO at Dumont d'Urville and Vostok, in Summer and Winter[a]

	DMS Lifetime	DMS	Sulfate	MSA	MSA + DMSO
Dumont d'Urville	3/5	3/5	9/10	9/23	7/12
Vostok	2/46	9/8	15/15	15/27	15/15

[a]Lifetimes are given in days. Entries are given as "summer/winter."

similar mean ages for sulfate and MSA in summer, but different in winter, which corroborates this result.

[49] Figure 9 shows the geographic origin of DMS leading to MSA and sulfate at Vostok, central Antarctica, in summer and in winter. In summer, the highest mean contributions are found at 55°–60°S, i.e., a little bit farther north than the sources related to Dumont d'Urville. In winter, the contributions are rather similar at both sites. Therefore there is basically no large difference between the two sites, as far as mean contributions are concerned. Nevertheless, the meridional distributions of the sources of MSA and sulfate display interannual variability much less marked at Vostok than at Dumont d'Urville. This is certainly due to the difference in the geographical situation of the stations. As the simulations were performed with nudging to reanalysis, the modeled atmospheric circulation displays realistic interannual variability. Meanwhile oceanic DMS concentrations are prescribed, so the modeled interannual variability of DMS fluxes is directly linked to variability in meteorology and sea ice cover. Results at Dumont d'Urville (Figure 8) display rather high interannual variability due to variability of meteorology. This is not the case for Vostok. Consequently, Vostok information would probably be mainly sensitive to the interannual variability of oceanic DMS concentrations, if it existed in the model. This has implications for the study of sulfur cycle in the general context of climate evolution studies: Long-term measurements of sulfur aerosols at inland Antarctic sites should provide more direct information on DMS concentrations at large spatial scales. Central Antarctic sites therefore might provide a more direct way to monitor the feedbacks of possible climate changes on marine biogenic activity than coastal Antarctic stations.

6.3. Age of Sulfur Species

[50] Ages of DMS, sulfate, and MSA, and DMS chemical lifetimes (computed during the forward simulations) at Dumont d'Urville and Vostok, in summer and winter, are reported in Table 3. Results for "MSA + DMSO" are also reported and discussed in section 6.4.

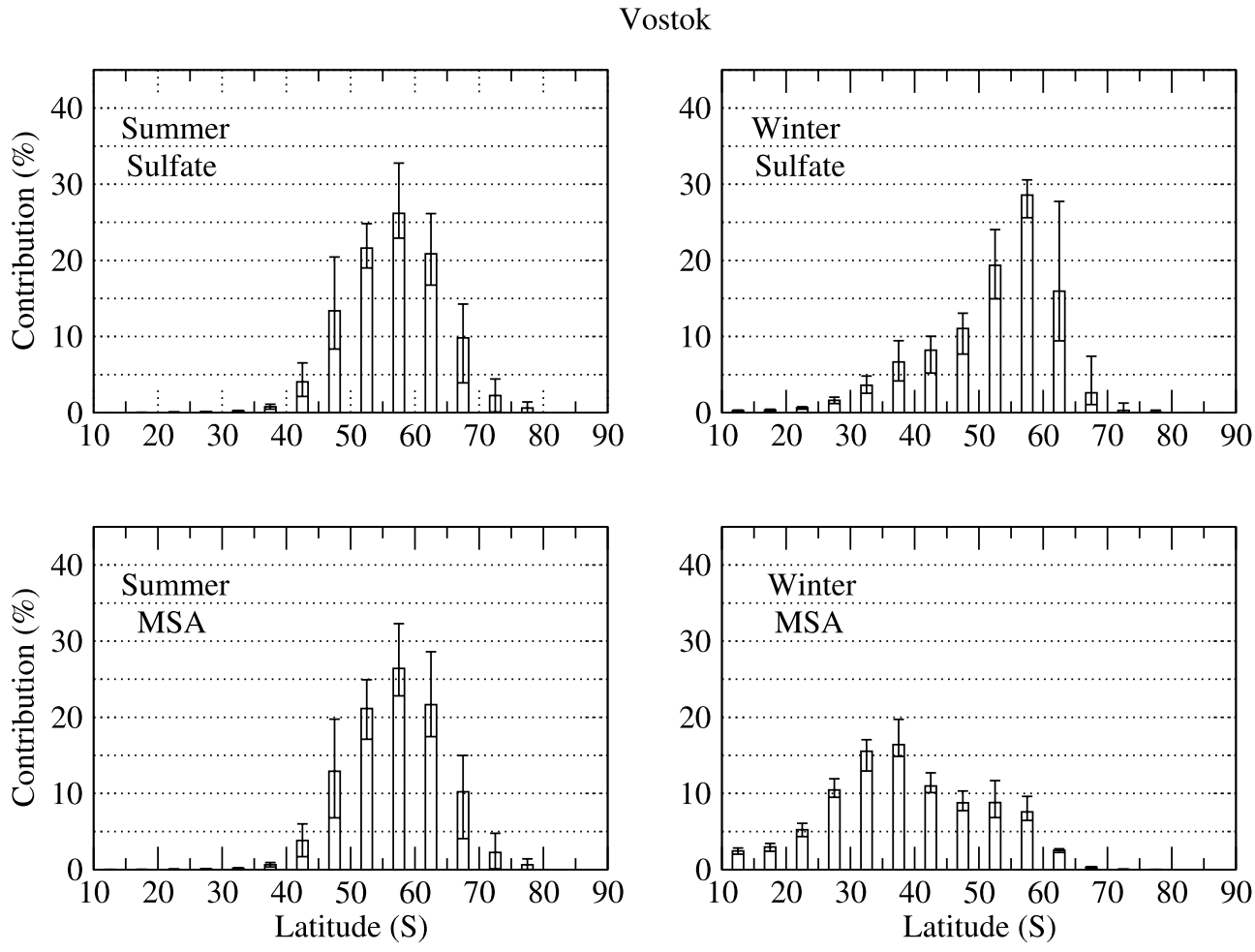

Figure 9. Same as Figure 8, but for Vostok.

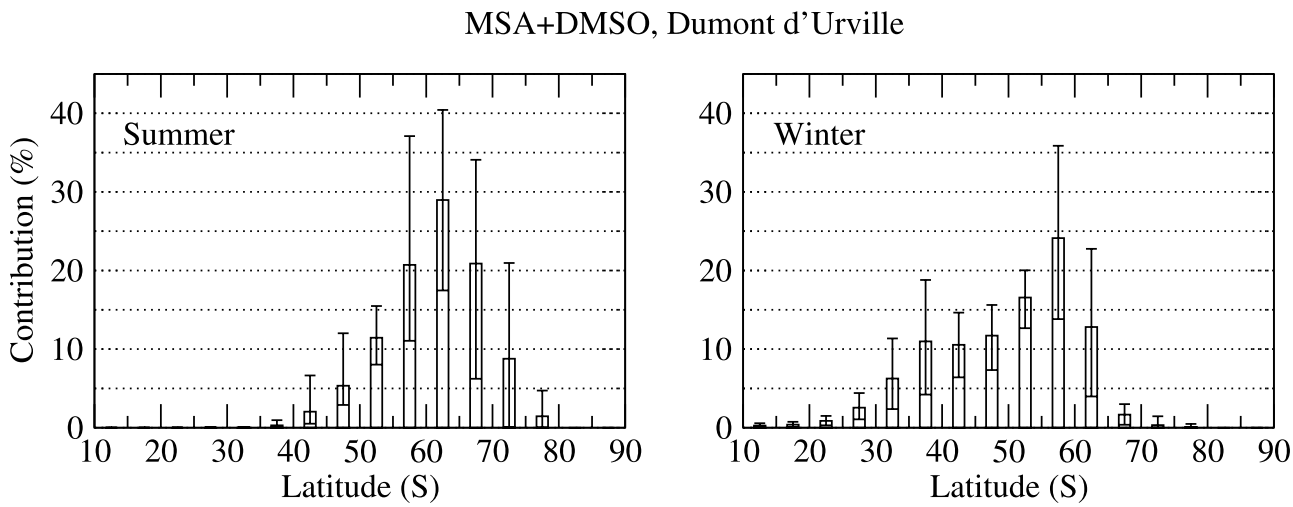

Figure 10. Meridional distribution, by 5° latitude bands, of the 5-year mean contributions of oceanic DMS sources to MSA + DMSO concentration at Dumont d'Urville, in summer and in winter. Error bars indicate minimum and maximum values among the 5 years.

6.3.1. DMS Ages/Lifetimes

[51] DMS lifetime represents DMS age if there was no other process than chemistry. At Dumont d'Urville, DMS ages and chemical lifetimes are similar. This corroborates the result from Figure 7 that DMS is essentially from local sources in summer. Transport has little influence. Winter case may appear misleading: DMS age and lifetime are similar, but DMS is not from purely local sources. In fact, in the 55°–60°S region (which especially influences DMS at Dumont d'Urville, Figure 7), DMS lifetime is only 3.5 days in July. Schematically, once transported to Dumont d'Urville from these latitudes, DMS appears to be 5 days old on average. At Vostok, DMS ages and lifetimes have nothing in common: The age is larger than the lifetime in summer (9 versus 2 days) and lower in winter (8 versus 46 days). Surprisingly, summer and winter ages are of the same order of magnitude, whereas chemical lifetimes differ by a factor of 20. This suggests that, as opposed to Dumont d'Urville, DMS age at Vostok is mainly driven by transport processes rather than chemistry.

6.3.2. Dumont d'Urville/Vostok

[52] Species are systematically older at Vostok. Obviously, this reflects the distance from the source. More precisely, sulfur species are 6–8 days older at Vostok than at Dumont d'Urville in summer, and 3–5 days older in winter. The smaller age difference between stations in winter than in summer is probably due to intensification of the atmospheric circulation in this season, as already mentioned in section 6.2. Because Dumont d'Urville is relatively close to the oceanic DMS sources all over the year, it is mostly sensitive to local sources and then weakly affected by changes in advection efficiency (except for MSA in winter). Vostok, farther away from the sources, is more affected.

6.3.3. Summer/Winter

[53] Basically, in winter, sulfur chemistry slows down and advection intensifies. The slowing down of DMS oxidation leads to higher ages in winter than in summer at Dumont d'Urville. The seasonal variations in chemistry affect the various species differently. Sulfate becomes only 1 day older, whereas MSA is 14 days older in winter at the coastal site. This is due to the DMS oxidation scheme, as explained in section 5.2. Seasonality of species ages at Vostok results from the complex coupling of seasonality of transport and chemistry. This coupling can lead to rather surprising results: DMS is slightly younger in winter than in summer (8 versus 9 days). Schematically, slower chemistry tends to "age" DMS, while intensified advection tends to make it "younger" in winter, and advection takes the lead. Seasonality at Vostok is well marked for MSA age, for which summer to winter change due to transport cannot compensate for the change due to chemistry.

6.4. Impacts of Model Defects

[54] The first important known model defect concerns DMSO oxidation: The chemistry module probably misses a significant process by which DMSO is scavenged by aerosols and oxidized into MSA in the particulate form [*Davis et al.*, 1998; *Legrand et al.*, 2001; *Cosme et al.*, 2002]. To get an upper limit of what would be the meridional origin and the age of MSA if this defect were corrected, we have considered the sum of MSA and DMSO (termed "MSA + DMSO" hereinafter), representing MSA if all DMSO was instantaneously converted into MSA. It is equivalent to most 3-D model results, which do not calculate DMSO. Figure 10 shows the geographic origin of DMS leading to MSA + DMSO at Dumont d'Urville, in summer and in winter. In summer, the meridional source profile does not strongly contrast with the profile for MSA alone (Figure 8): The contribution of each latitude band to MSA and MSA + DMSO never differs by more than 6% and MSA + DMSO is younger than MSA by only 2 days (Table 3). This is actually a consequence of the fast kinetics of DMSO oxidation into MSA by OH in the gas phase. An additional reaction of DMSO oxidation into MSA would fasten the local production of MSA but have little influence on remote sources. Indeed, in the case of Vostok (not shown), the profiles (and the ages) obtained with and without DMSO added to MSA are identical: Gaseous oxidation is sufficient to convert virtually all DMSO into MSA during transport. The case of winter is very different, for OH concentrations

are very low, and thus DMSO oxidation is very slow. Consequently, there is nearly no MSA in winter at Dumont d'Urville (*Cosme et al.* [2002], in agreement with the in situ observations of *Minikin et al.* [1998]) whereas DMSO is present [*Jourdain and Legrand*, 2001]. Thus MSA + DMSO is essentially DMSO. In fact the role of the reaction of DMSO oxidation onto the aerosol surface has not been clearly established in winter. It is probably not very active, since OH radicals are not formed during night time. Evaluating MSA + DMSO instead of MSA alone may thus be irrelevant in winter for our purpose. In any case, the results are qualitatively identical to the results for MSA only: MSA at Dumont d'Urville comes from sources located farther north than the sources of sulfate.

[55] The second model defect is an underestimation of DMSO in winter at Dumont d'Urville, possibly attributed to the lack, in the model, of a reaction of DMS oxidation by bromine oxide (BrO) that would lead to DMSO production. This is not likely to strongly affect the previous results, since in winter MSA formation from DMSO oxidation is nearly stopped.

[56] The third model defect likely to influence our calculations is the wet deposition scheme, probably not well adapted to polar precipitation: MSA and sulfate depositions are nearly systematically exaggerated. Because of its coastal location, Dumont d'Urville is little affected, but Vostok probably is. The effects of this defect are hardly quantifiable a priori, but are likely to induce moderate underestimations of distances to sources and ages: If deposition effects were reduced within the continent, MSA and sulfate would be less depleted in the retrotransport computation with the point source at Vostok, compared with the present computation. The concentrations of the sulfur species leaving the continent would be higher. The plumes formed would have larger lifetimes and would be retrotransported farther north. MSA and sulfate depletion due to chemistry, compared to deposition effects, would be increased, probably amplifying the differences between MSA and sulfate sources and ages. The plumes computed in the retrotransport integration would also be more diffused and widespread, blurring the interannual variability of MSA and sulfate sources. Thus the conclusions of section 6.2 probably remain valid, and might even be reinforced.

7. Summary

[57] This work aimed to provide a qualitative and quantitative description of the origin of sulfur species in the eastern Antarctic region. Such an inverse problem cannot be easily addressed with a direct three-dimensional modeling approach; adjoint methods are more adapted. We made use of a method of retrotransport already developed for the LMD-ZT GCM [*Hourdin and Issartel*, 2000; Hourdin et al., submitted manuscript, 2004], and extended here to account for sulfur chemistry. By releasing tracers at a measurement station, retrotransport enables one to calculate the sensitivities of this station to external parameters (initial field, lateral boundary conditions, emissions). Here, because we used a GCM and because we considered integration time intervals long enough to make the measurements insensitive to the initial conditions, we were only concerned with emissions. Knowing the emissions, it is possible to deconvolve, in terms of spatial distribution, history and types of sources, the various contributions to tracer concentrations simulated at the station.

[58] The retrotransport method was used to find how transport and chemistry affect the sulfur cycle observed at Dumont d'Urville, then to find the origin of DMS, sulfate and MSA at Dumont d'Urville and Vostok. Dumont d'Urville is on the coast and strongly influenced by katabatic winds from the continent. However, since there are very few sources south of Dumont d'Urville, the sulfur cycle is mainly driven by the oceanic DMS emissions. More than 90% of sulfur compounds in eastern Antarctica originate from the ocean.

[59] The inland regions, although farther away from the midlatitudes, seem to be relatively more affected by anthropogenic and volcanic sources than the coastal regions. Inland regions are probably more directly affected by long-range transport of pollutants occurring in the middle/high troposphere. However, the regions near the Ross sea may sometimes receive emissions from Mount Erebus, the only volcano accounted for in the model that is active in the Antarctic region; Dumont d'Urville can be affected by these emissions.

[60] MSA and sulfate aerosols have the same geographical origin and the same age in summer. This is due to the similar kinetics of their respective production from DMS oxidation by OH. However, in winter, MSA comes from farther north than sulfate, and is thus older: Sulfate continues to be produced in the absence of OH during the polar night, while MSA production is stopped.

[61] Vostok also appears influenced by oceanic DMS emissions. However, unlike Dumont d'Urville, for which interannual variability is high, the locations of DMS emissions that influence Vostok display very low interannual variations. In our model, variations of DMS fluxes are due only to variations in meteorology, not in the water DMS concentrations. This suggests that sulfur species monitoring at inland scientific stations may be particularly useful for monitoring large-scale interannual variations in water DMS content, and the long-term interactions between climate and the natural sulfur cycle.

[62] Two effects compete to control the summer/winter differences in the age of sulfur species: the winter intensification of the atmospheric circulation and the slowing down of chemical kinetics. At Dumont d'Urville, the effect of slower chemistry dominates for all species, which are older in winter. At Vostok, only MSA follows this rule whereas sulfate appears 15 days old in both summer and winter and DMS is slightly younger in winter than in summer. Finally, we showed that known model defects concerning the sulfur cycle are not likely to drastically affect the results of this work.

[63] **Acknowledgments.** We thank Michel Legrand and Bruno Jourdain for the fruitful discussions that motivated and helped us in this work. Computer time was provided by the Centre Grenoblois de Calcul Vectoriel (CGCV) of the Commissariat à l'Energie Atomique (CEA) and by the Institut du Développement et des Ressources en Informatique Scientifique (IDRIS). Sea surface temperature maps used as boundary conditions in the GCM come from the Met Office (GISST data). This work is part of a research project supported by the Programme National de Chimie Atmosphrique (PNCA) of the Institut National des Sciences de l'Univers (INSU) and by the Institut Polaire Français Paul-Emile Victor (IPEV) and was inspired by the European Project of Ice Coring in Antarctica (EPICA). The first version of the manuscript has been greatly improved thanks to the helpful comments of two anonymous reviewers.

References

Albrecht, B. A. (1989), Aerosols, cloud microphysics, and fractional cloudiness, *Science*, *245*, 1227–1230.

Andreae, M. (1986), The ocean as a source of atmospheric sulfur compounds, in *The Role of Air-Sea Exchange in Geochemical Cycling*, edited by P. Buat-Ménard, pp. 331–362, Springer, New York.

Andreae, M. O., and T. W. Andreae (1988), The cycle of biogenic sulfur compounds over the Amazon basin: 1, Dry season, *J. Geophys. Res.*, *93*, 1487–1497.

Andreae, M. O., H. Berresheim, H. Bingemer, D. J. Jacob, B. L. Lewis, S. M. Li, and R. W. Talbot (1990), The atmospheric sulfur cycle over the Amazon basin: 2, Wet season, *J. Geophys. Res.*, *95*, 16,813–16,824.

Andres, R. J., and A. D. Kasgnoc (1998), A time-averaged inventory of subaerial volcanic sulfur emissions, *J. Geophys. Res.*, *103*, 25,251–25,261.

Bates, T. S., B. K. Lamb, A. Guenther, J. Dignon, and R. E. Stoiber (1992), Sulfur emissions from natural sources, *J. Atmos. Chem.*, *14*, 315–337.

Benkovitz, C. M., C. M. Berkowitz, R. C. Easter, S. Nemesure, R. Wagener, and S. E. Schwartz (1994), Sulfate over the North Atlantic and adjacent continental regions: Evaluation for October and November 1986 using a three-dimensional model driven by observation-derived meteorology, *J. Geophys. Res.*, *99*, 20,725–20,756.

Benkovitz, C. M., M. T. Scholtz, J. Pacyna, L. Tarrasón, J. Dignon, E. C. Voldner, P. A. Spiro, J. A. Logan, and T. E. Graedel (1996), Global gridded inventories of anthropogenic emissions of sulfur and nitrogen, *J. Geophys. Res.*, *101*, 29,239–29,253.

Berresheim, H., and F. L. Eisele (1998), Sulfur Chemistry in the Antarctic Troposphere Experiment: An overview of project SCATE, *J. Geophys. Res.*, *103*, 1619–1627.

Boucher, O., and U. Lohmann (1995), The sulphate-CCN-cloud albedo effect: A sensitivity study with two general circulation models, *Tellus, Ser. B*, *47*, 281–300.

Boucher, O., M. Pham, and C. Venkataraman (2002), Simulation of the atmospheric sulfur cycle in the Laboratoire de Mtorologie Dynamique general circulation model: Model description, model evaluation, and global and European budgets, *Note Sci. de l'IPSL 23*, Inst. Pierre-Simon Laplace, Paris.

Challenger, F. (1951), Biological methylation, *Adv. Enzymol.*, *12*, 429–491.

Charlson, R. J., J. E. Lovelock, M. O. Andreae, and S. G. Warren (1987), Oceanic phytoplankton, atmospheric sulphur, cloud albedo and climate, *Nature*, *326*, 655–661.

Chin, M., D. L. Savoie, B. J. Huebert, A. R. Bandy, D. C. Thornton, T. S. Bates, P. K. Quinn, E. S. Saltzman, and W. J. De Bruyn (2000), Atmospheric sulfur cycle simulated in the global model GOCART: Comparison with field observations and regional budgets, *J. Geophys. Res.*, *105*, 24,689–24,712.

Cosme, E. (2002), *Cycle du soufre des moyennes et hautes latitudes Sud dans un modèle de circulation générale atmosphérique*, 250 pp., Ph.D. thesis, Univ. Joseph Fourier–Grenoble I, Grenoble, France.

Cosme, E., C. Genthon, P. Martinerie, O. Boucher, and M. Pham (2002), The sulfur cycle at high-southern latitudes in the LMD-ZT general circulation model, *J. Geophys. Res.*, *107*(D23), 4690, doi:10.1029/2002JD002149.

Davis, D., G. Chen, P. Kasibhatla, A. Jefferson, D. Tanner, F. Eisele, D. Lenschow, W. Neff, and H. Berresheim (1998), DMS oxidation in the Antarctic marine boundary layer: Comparison of model simulations and field observations of DMS, DMSO, $DMSO_2$, H_2SO_4 (g), MSA (g), and MSA (p), *J. Geophys. Res.*, *103*, 1657–1678.

Delmas, R., and J. Servant (1983), Atmospheric balance of sulfur above an equatorial forest, *Tellus, Ser. B*, *35*, 110–120.

Flesch, T. K., J. D. Wilson, and E. Yee (1995), Backward-time Lagrangian stochastic dispersion model and their application to estimate gaseous emissions, *J. Appl. Meteorol.*, *34*, 1320–1333.

Genthon, C., G. Krinner, and E. Cosme (2002), Free and laterally-nudged Antarctic climate of an atmospheric general circulation model, *Mon. Weather Rev.*, *130*, 1601–1616.

Guenther, A. B., B. K. Lamb, and H. H. Westberg (1989), U.S. National biogenic sulfur emissions inventory, in *Biogenic Sulfur in the Environment*, *ACS Symp. Ser.*, vol. 393, edited by E. Saltzman and W. Cooper, pp. 14–30, Am. Chem. Soc., Washington, D. C.

Hauglustaine, D., F. Hourdin, L. Jourdain, M. Filiberti, S. Walters, J. Mararque, and E. A. Holland (2004), Interactive chemistry in the Laboratoire de Météorologie Dynamique general circulation model: Description and background tropospheric chemistry evaluation, *J. Geophys. Res.*, *109*, D04314, doi:10.1029/2003JD003957.

Hourdin, F., and A. Armengaud (1999), The use of finite-volume methods for atmospheric advection of trace species. part i: Test of various formulations in a general circulation model, *Mon. Weather Rev.*, *127*, 822–837.

Hourdin, F., and J.-P. Issartel (2000), Sub-surface nuclear tests monitoring through the CTBT xenon network, *Geophys. Res. Lett.*, *27*, 2245–2248.

Hourdin, F., J.-P. Issartel, B. Cabrit, and A. Idelkadi (1999), Reciprocity of atmospheric transport of trace species, *C. R. Acad. Sci., Ser. IIa*, *329*, 623–628.

James, I. N. (1989), The Antarctic drainage flow: Implications for hemispheric flow on the Southern Hemisphere, *Antarct. Sci.*, *1*, 279–290.

Jourdain, B., and M. Legrand (2001), Seasonal variations of atmospheric dimethylsulfide, dimethylsulfoxide, sulfur dioxyde, methanesulfonate and non-sea-salt sulfate aerosols at Dumont d'Urville (coastal Antarctica) (December 1998–July 1999), *J. Geophys. Res.*, *106*, 14,391–14,407.

Kettle, A. J., and M. O. Andreae (2000), Flux of dimethylsulfide from the oceans: A comparison of updated data sets and flux models, *J. Geophys. Res.*, *105*, 26,793–26,808.

Kettle, A. J., et al. (1999), A global database of sea surface dimethylsulfide (DMS) measurements and a procedure to predict sea surface DMS as function of latitude, longitude and month, *Global Biogeochem. Cycles*, *13*, 399–444.

King, J., and J. Turner (1997), *Antarctic Meteorology and Climatology*, 409 pp., Cambridge Univ. Press, New York.

Koga, S., and H. Tanaka (1996), Simulations of seasonal variations of sulfur compounds in the remote marine atmosphere, *J. Atmos. Chem.*, *23*, 163–192.

König-Langlo, G., J. C. King, and P. Pettré (1998), Climatology of the three coastal Antarctic stations Dumont d'Urville, Neumayer, and Halley, *J. Geophys. Res.*, *103*, 10,935–10,946.

Kottmeier, C., and B. Fay (1998), Trajectories in the antarctic lower troposphere, *J. Geophys. Res.*, *103*, 10,947–10,960.

Krinner, G., and C. Genthon (2003), Tropospheric transport of continental tracers towards Antarctica under varying climatic conditions, *Tellus, Ser. B*, *55*, 54–70.

Krinner, G., C. Genthon, Z. Li, and P. Le Van (1997), Studies of the Antarctic climate with a stretched-grid general circulation model, *J. Geophys. Res.*, *102*, 13,731–13,745.

Legrand, M. (1997), Ice core records of atmospheric sulphur, *Philos. Trans. R. Soc. London, Ser. B*, *352*, 241–250.

Legrand, M., and C. Feniet-Saigne (1991), Methanesulfonic acid in South Pole snow layers: A record of strong El Nino?, *Geophys. Res. Lett.*, *18*, 187–190.

Legrand, M., and E. C. Pasteur (1998), Methane sulfonic acid to non-sea-salt sulfate ratio in coastal Antarctic aerosol and surface snow, *J. Geophys. Res.*, *103*, 10,991–11,006.

Legrand, M., J. Sciare, B. Jourdain, and C. Genthon (2001), Sub-daily variations of atmospheric dimethylsulfide, dimethylsulfoxide, methanesulfonate and non-sea-salt sulfate aerosols in the atmospheric boundary layer at Dumont d'Urville (coastal Antarctica) during summer, *J. Geophys. Res.*, *106*, 14,409–14,422.

Liss, P. S., and L. Merlivat (1986), Air-sea exchange rates: Introduction and synthesis, in *The Role of Air-Sea Exchange in Geochemical Cycling*, edited by P. Buat-Ménard, pp. 113–127, Springer, New York.

Mauldin, R. L., F. L. Eisele, D. J. Tanner, and E. Kosciuch (2001), Measurements of OH, H_2SO_4, and MSA at the South Pole during ISCAT, *Geophys. Res. Lett.*, *28*, 3629–3632.

McCormick, R. A., and H. Ludwig (1967), Climate modification by atmospheric aerosols, *Science*, *156*, 1358–1359.

Minikin, A., M. Legrand, J. Hall, D. Wagenbach, C. Kleefeld, E. Wolff, E. C. Pasteur, and F. Ducroz (1998), Sulfur-containing species (sulfate and methanesulfonate) in coastal Antarctic aerosol and precipitation, *J. Geophys. Res.*, *103*, 10,975–10,990.

Müller, J. (1992), Geographical distribution and seasonal variation of surface emissions and deposition velocities of atmospheric trace gases, *J. Geophys. Res.*, *97*, 3787–3804.

Müller, J., and G. P. Brasseur (1995), IMAGES: A three-dimensional chemical transport model of the global troposphere, *J. Geophys. Res.*, *100*, 16,455–16,490.

Nguyen, B. C., S. Belviso, N. Mihalopoulos, J. Gostan, and P. Nival (1988), Dimethyl sulphide production during natural phytoplankton blooms, *Mar. Chem.*, *24*, 133–141.

Penner, J. E., et al. (2001), Aerosols, their direct and indirect effects, in *Climate Change 2001: The Scientific Basis, Contribution of Working Group I to the Third Assessment Report of the Intergovernmental Panel on Climate Change*, edited by J. T. Houghton et al., chap. 5, pp. 289–348, Cambridge Univ. Press, New York.

Petit, J. R., et al. (1999), Climate and atmospheric history of the past 42,0000 years from the Vostok ice core, Antarctica, *Nature*, *399*, 429–436.

Pham, M., J. Müller, G. P. Brasseur, C. Granier, and G. Mégie (1995), A 3D model of the global sulfur cycle, *J. Geophys. Res.*, *100*, 26,061–26,092.

Seibert, A., and A. Frank (2003), Source-receptor matrix calculation with a Lagrangian particle dispersion model in backward mode, *Atmos. Chem. Phys. Discuss.*, *3*, 4515–4548.

Shaw, G. E. (1983), Bio-controlled thermostasis involving the sulfur cycle, *Clim. Change*, *5*, 297–303.

Spiro, P. A., D. J. Jacob, and J. A. Logan (1992), Global inventory of sulphur emissions with 1 × 1 resolution, *J. Geophys. Res.*, *97*, 6023–6036.

Tiedtke, M. (1989), A comprehensive mass flux scheme for cumulus parameterization in large-scale models, *Q. J. R. Meteorol. Soc.*, *117*, 1779–1800.

Toumi, R. (1994), BrO as a sink for dimethylsulfide in the marine atmosphere, *Geophys. Res. Lett.*, *21*, 117–120.

Twomey, S. A. (1974), Pollution and the planetary albedo, *Atmos. Environ.*, *8*, 1251–1256.

Van Leer, B. (1977), Towards the ultimate conservative difference scheme: IV. A new approach to numerical convection, *J. Comput. Phys.*, *23*, 276–299.

Watts, S. F. (2000), The mass budgets of carbonyl sulfide, dimethylsulfide, carbon disulfide and hydrogen sulfide, *Atmos. Environ.*, *34*, 761–779.

White, F. D.J., and R. A. Bryson (1967), The radiative factor in the mean meridional circulation of the antarctic atmosphere during the polar night, in *Polar Meteorology: Proceedings of the WMO/SCAR/ICPM Symposium on Polar Meteorology, Geneva, 5–9 September 1966*, *WMO Tech. Note 87*, pp. 199–224, World Meteorol. Organ., Geneva.

Wolff, E. W., M. R. Legrand, and D. Wagenbach (1998), Coastal Antarctic aerosol and snowfall chemistry, *J. Geophys. Res.*, *103*, 10,927–10,934.

E. Cosme, Department of Atmospheric and Oceanic Sciences, McGill University, 805 Sherbrooke Street West, Montreal, Quebec, Canada H3A 2K6. (emmanuel.cosme@mail.mcgill.ca)

C. Genthon and P. Martinerie, Laboratoire de Glaciologie et Géophysique de l'Environnement, 54 rue Molière, B. P. 96, F-38402, Saint-Martin-d'Hères Cedex, France.

F. Hourdin, Laboratoire de Météorologie Dynamique, CNRS/UPMC, Tour 25 Jussieu, Boite 99, F-75252 Paris Cedex 05, France.

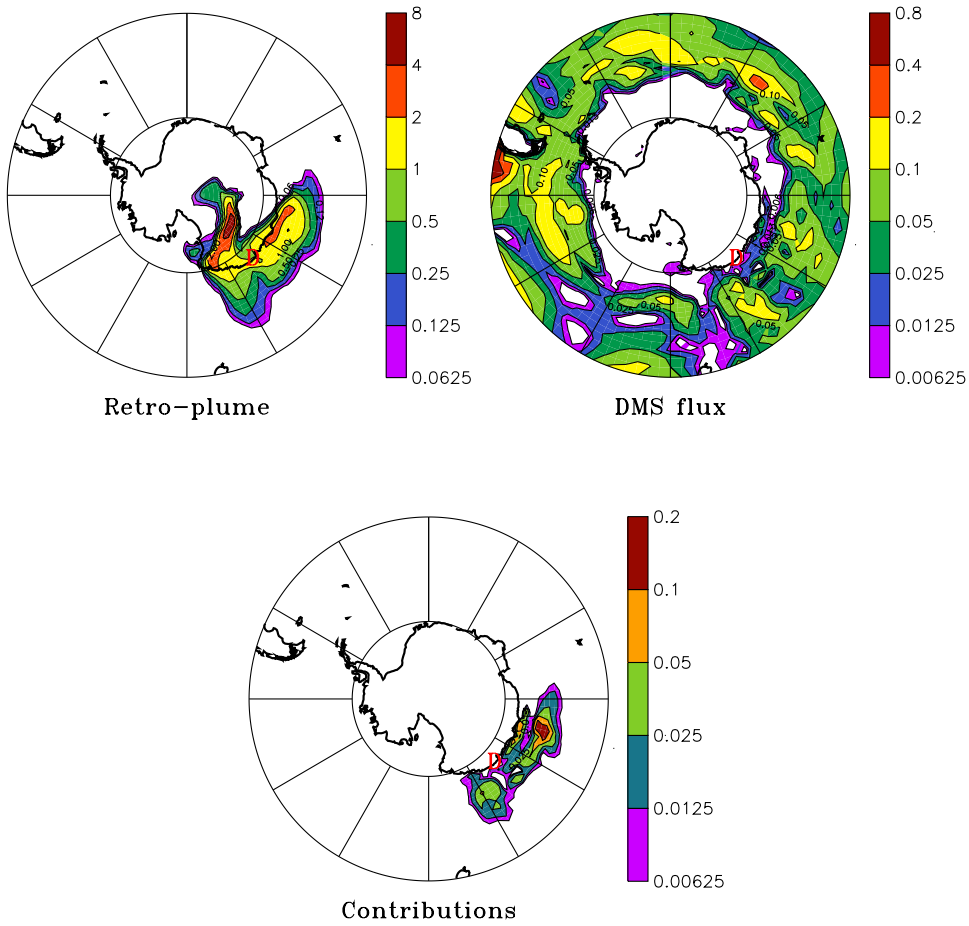

Figure 3. Retroplume of DMS in the first model layer on 27 July 1999, generated by a release of sulfate at Dumont d'Urville on 30 July (units: molecules per 10 km^3) (upper left map); oceanic DMS flux on 27 July (units: mg sulfur m^{-2} d^{-1}) (upper right map); contributions of DMS sources of 27 July to sulfate at Dumont d'Urville on 30 July (units are percent per 100 km^2) (bottom map). Dumont d'Urville is indicated by "D."

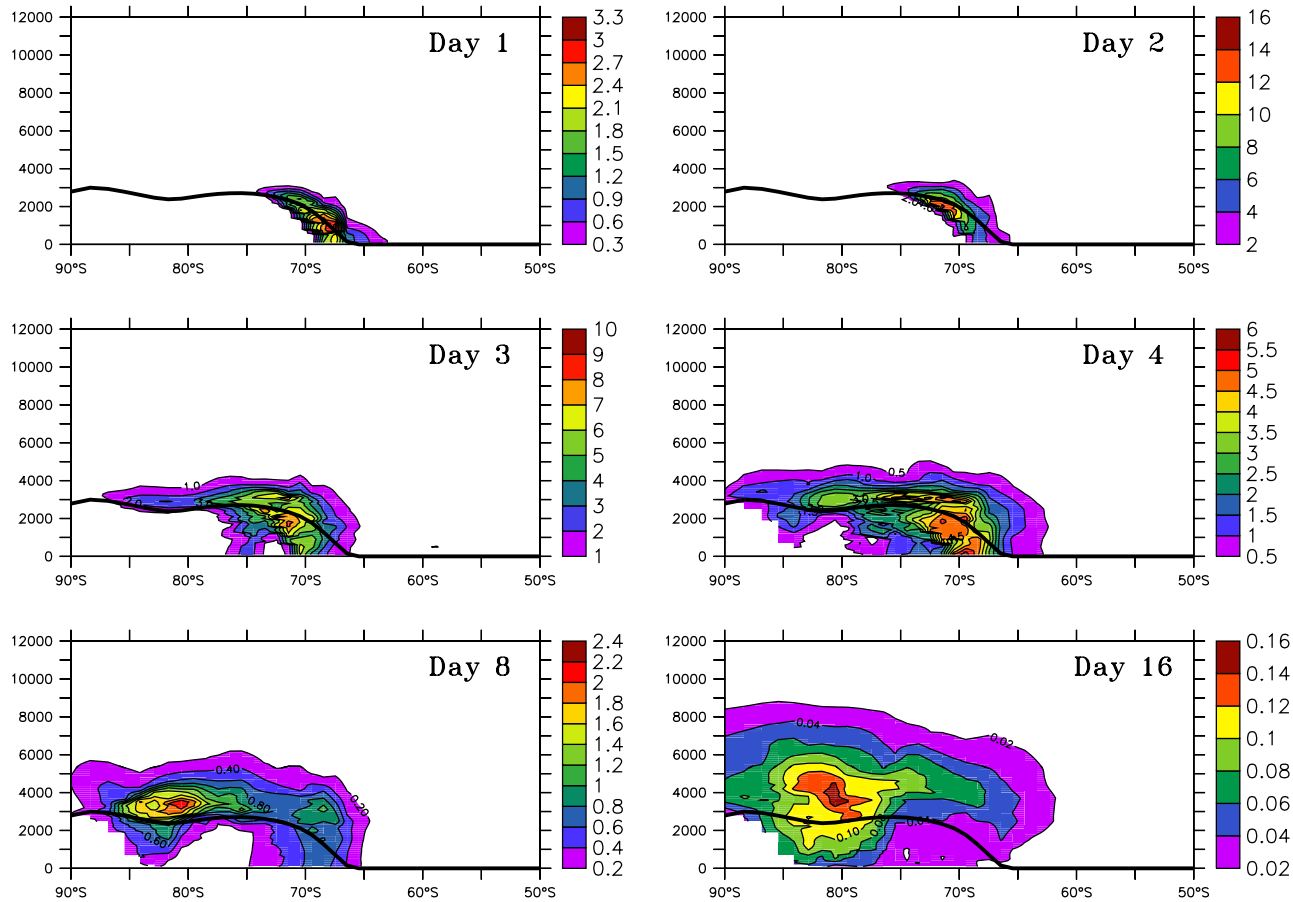

Figure 4. Vertical section (maximum values along the longitudes) of the 5-year mean retroplume of DMS generated by a release of sulfate at Dumont d'Urville (located on the coast, at 66°40′S) in January. Units are molecules per 10 km^3 volume, with 86,400 molecules having been released. "Day 1" refers to the day of release, "day 2" refers to the day before, and so on. The thick line roughly reproduces the minimal altitude of the ice cap between 130° and 150°E, where the coastal station is located.

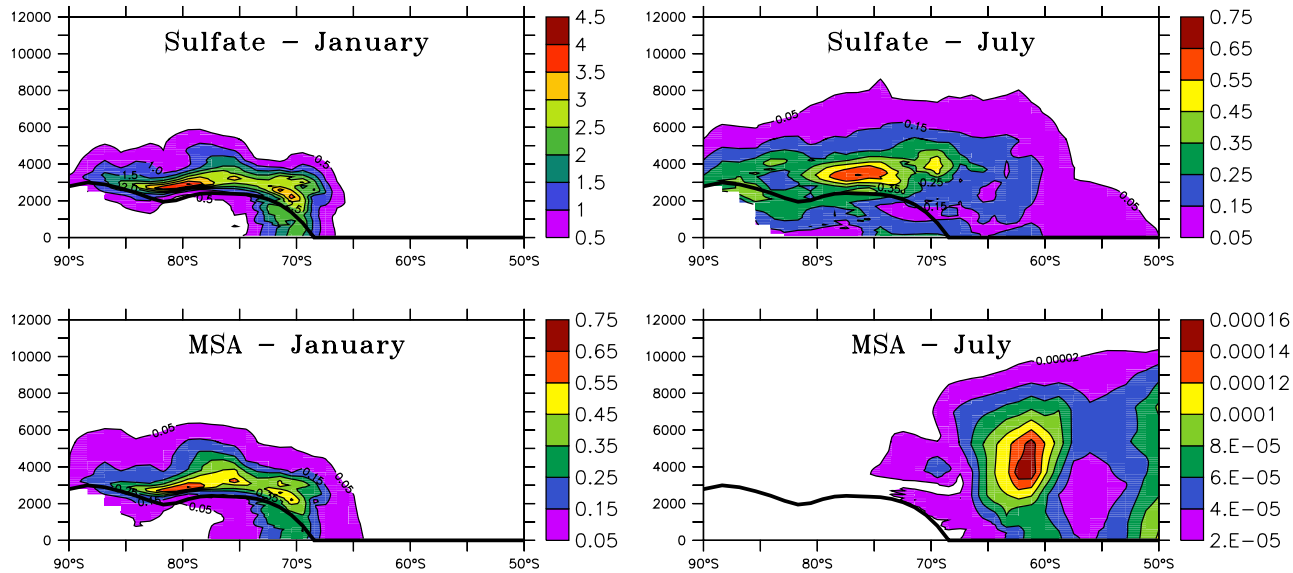

Figure 5. Vertical sections (maximum values along the longitudes) of the 5-year mean retroplumes of DMS, 5 days after releasing sulfate (upper panels) or MSA (lower panels), in (left) January or (right) July, at Dumont d'Urville.

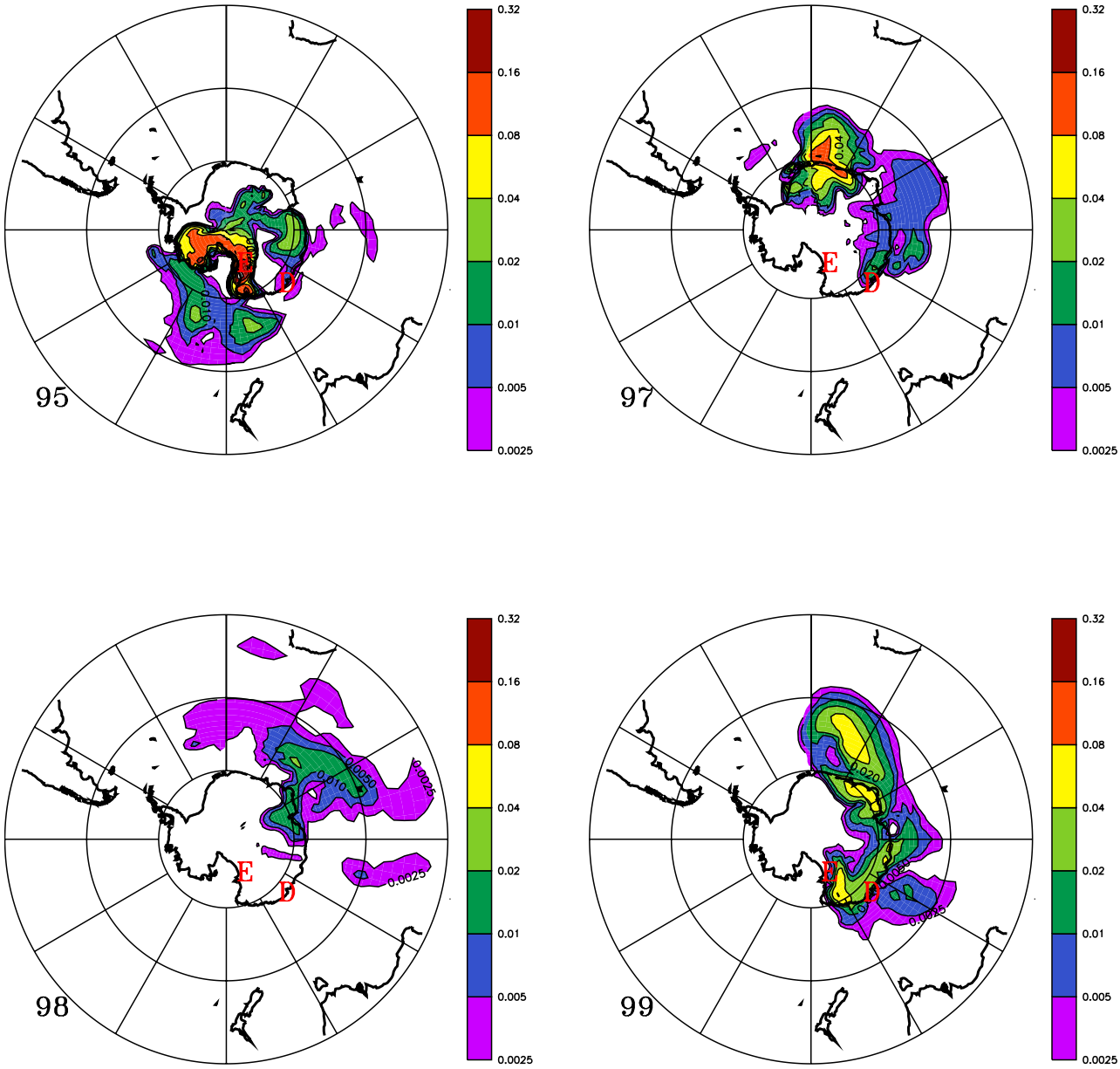

Figure 6. Retroplumes of SO_2 (in the first model layer), 3 days after a release of sulfate at Dumont d'Urville in July, for the years 1995 and 1997–1999. Dumont d'Urville is indicated by "D," and Mount Erebus is indicated by "E."